Fluids and Barriers of the CNS

RESEARCH

Open Access

Plasma S100β is a predictor for pathology and cognitive decline in Alzheimer's disease

Geetika Nehra[1], Bryan J. Maloney[1], Rebecca R. Smith[1], Wijitra Chumboatong[1], Erin L. Abner[1,2,3], Peter T. Nelson[1,4], Björn Bauer[1,5] and Anika M. S. Hartz[1,6*]

Abstract

Background Blood–brain barrier dysfunction is one characteristic of Alzheimer's disease (AD) and is recognized as both a cause and consequence of the pathological cascade leading to cognitive decline. The goal of this study was to assess markers for barrier dysfunction in postmortem tissue samples from research participants who were either cognitively normal individuals (CNI) or diagnosed with AD at the time of autopsy and determine to what extent these markers are associated with AD neuropathologic changes (ADNC) and cognitive impairment.

Methods We used postmortem brain tissue and plasma samples from 19 participants: 9 CNI and 10 AD dementia patients who had come to autopsy from the University of Kentucky AD Research Center (UK-ADRC) community-based cohort; all cases with dementia had confirmed severe ADNC. Plasma samples were obtained within 2 years of autopsy. Aβ40, Aβ42, and tau levels in brain tissue samples were quantified by ELISA. Cortical brain sections were cleared using the X-CLARITY™ system and immunostained for neurovascular unit-related proteins. Brain slices were then imaged using confocal microscopy and analyzed for microvascular diameters and immunoreactivity coverage using Fiji/ImageJ. Isolated human brain microvessels were assayed for tight-junction protein expression using the JESS™ automated Western blot system. S100 calcium-binding protein B (S100β), matrix metalloproteinase (MMP)-2, MMP-9, and neuron-specific enolase (NSE) levels in plasma were quantified by ELISA. All outcomes were assessed for linear associations with global cognitive function (MMSE, CDR) and cerebral atrophy scores by Pearson, polyserial, or polychoric correlation, as appropriate, along with generalized linear modeling or generalized linear mixed-level modeling.

Results As expected, we detected elevated Aβ and tau pathology in brain tissue sections from AD patients compared to CNI. However, we found no differences in microvascular diameters in cleared AD and CNI brain tissue sections. We also observed no differences in claudin-5 protein levels in capillaries isolated from AD and CNI tissue samples. Plasma biomarker analysis showed that AD patients had 12.4-fold higher S100β plasma levels, twofold lower NSE plasma levels, 2.4-fold higher MMP-9 plasma levels, and 1.2-fold lower MMP-2 plasma levels than CNI. Data analysis revealed that elevated S100β plasma levels were predictive of AD pathology and cognitive impairment.

Conclusion Our data suggest that among different markers relevant to barrier dysfunction, plasma S100β is the most promising diagnostic biomarker for ADNC. Further investigation is necessary to assess how plasma S100β levels relate to these changes and whether they may predict clinical outcomes, particularly in the prodromal and early stages of AD.

Keywords Blood–brain barrier, Aβ, Tau, MMSE

*Correspondence:
Anika M. S. Hartz
anika.hartz@uky.edu
Full list of author information is available at the end of the article

Background

Alzheimer's disease (AD) is the most common form of dementia. AD neuropathologic change (ADNC) is characterized by beta-amyloid (Aβ) plaque deposition and hyperphosphorylated microtubule-associated protein tau (tau) aggregation [1]. A result of these pathological changes in patients is cognitive decline that is usually not clinically noticeable until years after pathology onset [2]. While over 140 unique interventions are tested for safety and efficacy in more than 180 AD clinical trials, only 7 FDA-approved drugs are currently available for AD patients [1, 3]. Four drugs, donepezil, galantamine, rivastigmine, and memantine, provide modest cognitive improvements that diminish after 6–12 months [4]. Three recent amyloid-targeting antibodies (aducanumab (withdrawn from the market in January 2024), lecanemab, and donanemab) reduce Aβ pathology and delay the progression of cognitive decline by about 6 months after 18 months of treatment [5, 6]. However, both Aβ-directed antibodies can induce brain edema and microhemorrhages, and any therapeutic advantage remains to be verified in large patient cohorts [5–8]. Importantly, patients need to be diagnosed early to benefit from these new Aβ-targeting therapies. Thus, identifying noninvasive biomarkers to detect AD pathology and predict cognitive impairment early remains a critical clinical need.

Current diagnostic tools for AD include positron emission tomography scans with Aβ and tau tracers, laboratory tests to determine Aβ42/Aβ40 ratios or tau protein levels in the cerebrospinal fluid, magnetic resonance imaging (MRI) scans to visualize brain structural changes, neurological exams, and memory tests [8–11]. Recently, blood–brain barrier dysfunction has emerged as an early and prominent sign associated with neurodegeneration and cognitive impairment in elderly individuals and patients with early AD [10–19]. AD pathology alters blood–brain barrier structure and biochemistry, leading to barrier dysfunction. This dysfunction can be detected as cerebral microbleeds in susceptibility-weighted MRI scans and elevated permeability coefficients in dynamic contrast-enhanced MRI scans [3, 10, 11]. Barrier dysfunction has been detected by immunohistochemical analysis of extravasated proteins in postmortem brain slices [13, 14, 18–21]. Barrier dysfunction precedes cognitive decline in AD patients, pointing to barrier-associated biomarkers as a potential tool for early detection of AD neuropathologic changes [22]. In the present study, we analyzed postmortem tissue samples from cognitively normal individuals (CNI) and individuals with AD pathology for signs of blood–brain barrier dysfunction and correlated our findings with ADCN and cognitive impairment. The objective of this study was to determine if markers for blood–brain barrier dysfunction are associated with AD pathology and cognitive impairment.

Methods

Human brain tissue samples

Postmortem brain tissue samples (frontal cortex, Brodmann area 9) and plasma samples were obtained from the University of Kentucky Alzheimer's Disease Research Center (UK-ADRC) Brain Bank (IRB protocol #B18-3115-M4). Briefly, research participants enrolled in the UK-ADRC longitudinal cohort and were followed approximately annually until death. Annual assessments include mental status testing, physical examination, medical history, neurological examination, and provision of blood samples. Participants were recruited using community-based cohort methods, which have been described previously [23]. Sample size was based on preliminary data in mouse and human capillaries and availability [20]. Inclusion criteria for the current study consisted of a clinicopathologic consensus diagnosis of normal cognition (cognitively normal individual (CNI)) or AD dementia, available blood draw within two years of death, a postmortem interval of less than 4 h, and the presence of mild-to-severe cerebral amyloid angiopathy (CAA), a driver of barrier leakage (Table 1; [20]. Participants with Diffuse Lewy Body Disease and/or a history of seizures were excluded.

Neuropathology of brain tissue samples

Paraffin-embedded tissue samples were sectioned into 8 μm slices and stained for diffuse Aβ plaques (DPs), neuritic Aβ plaques (NPs), and neurofibrillary tangles (NFTs) using a modified Bielschowsky method [24–28]. DP refers to plaques with "*loose structures with irregular and ill-defined margin*"; NP refers to plaques with "*clear-cut outlines and a neuritic core*" [29, 30]. DPs were quantified across 5 fields of view (field size: 2.35 mm^2) with an arbitrary threshold of 250 plaques over all 5 fields. NPs were quantified without a preset threshold. NFTs were quantified across 5 fields of view that were manually determined to be most severely affected (field size: 0.586 mm^2). Mean DP, NP, and NFT numbers were calculated for each brain. CAA severity was categorized as mild (1), moderate (2), or severe (3) from Aβ40-immunostained brain tissue sections based on criteria adapted from previous studies [31–33]. Mild CAA (severity score 1) was defined as scattered positivity in parenchymal and/or leptomeningeal vessels, possibly in only one brain area. Moderate CAA (severity score 2) referred to positivity in many parenchymal and leptomeningeal vessels. Severe CAA (severity score 3) referred to widespread and intense positivity in parenchymal and leptomeningeal vessels.

Table 1 Characteristics of included cases (N = 19)

Neuropathological Outcomes	CNI (*n* = 9)	AD (*n* = 10)
Age (y, mean ± SD)	86.7 ± 6.0	82.2 ± 9.0
PMI (h, mean ± SD)	3.6 ± 3.4	3.9 ± 1.5
Duration		
Gender (M/F)	4/5	3/7
Race	White	White
Education (y, mean ± SD)	16.1 ± 1.5	14.0 ± 2.9
APOE allele status		
e3/e3	3	4
e2/e3	3	0
e3/e4	2	4
e4/e4	1	2
CDRGLOB	0–0	0.5–3
MMSE score (mean ± SD)	29.1 ± 1.3	18.0 ± 9.5
Braak staging	I–III	V–VI
CAA	1–3	1–3
Co-morbidities		
Cancer	5	3
Smoking	4	3
Heart attack	2	0
Atrial fibrillation	1	1
Hypertension	5	4
Transient ischemic attack	0	1
Cardiac arrythmia	2	1
Diabetes	0	1
Cerebral atrophy	Abs/mild/mod	Abs/mild/mod

Cortical atrophy (CA) was determined by gross examination of the postmortem brain tissue. CA severity was categorized as mild (1), moderate (2), or severe (3), consistent with the National Alzheimer's Coordination Center ordinal scale [34].

Aβ extraction

Snap-frozen (liquid nitrogen) brain tissue samples from deceased AD patients, and CNI were weighed and homogenized in 0.4 mL extraction buffer A (5 M guanidine-HCl (G3272); 50 mM Tris HCl (T0819), Millipore-Sigma, Burlington, MA, USA). Homogenates were diluted in extraction buffer B (DBPS (D5652); 5% BSA (A9647, Millipore-Sigma, Burlington, MA, USA) containing 1 × Protease Inhibitor Cocktail Set 1 (539131, Millipore-Sigma, Burlington, MA, USA, 1:100 dilution) and centrifuged (16,000 g, 20 min, 4 °C) to obtain supernatants for Aβ ELISAs.

Tau extraction

Snap-frozen (liquid nitrogen) tissue samples were weighed and homogenized in 10 volumes of 1 × Cell Extraction Buffer PTR provided in the ELISA kit (ab273617, Abcam, Cambridge, MA, USA) and contained 1 × Protease Inhibitor Cocktail Set 1 (539131, Millipore-Sigma, Burlington, MA, USA; 1:100 dilution). Samples were centrifuged (18,000 g, 20 min, 4 °C) to obtain supernatants for Tau ELISA.

ELISA for S100β, Iba-1, caveolin-1, MMP-2, MMP-9, NSE, Aβ40, Aβ42 and Tau

Samples were analyzed for various analytes using commercially available ELISA kits per the manufacturers' instructions. Plasma samples were analyzed for S100β protein using human S100β ELISA kit (EZHS100B-33 K, Millipore-Sigma, Burlington, MA, USA). Iba-1 was determined using Novus Human AIF-1/Iba1 ELISA Kit #NBP2-66674 (Novus Biologicals, Centennial, CO, USA). Caveolin-1 was measured with Human Caveolin-1 SimpleStep ELISA Kit (ab318937, Abcam, Cambridge, MA, USA). MMP-2 protein using MMP-2 ELISA kit (MMP200, R&D Systems, Minneapolis, MN, USA), MMP-9 protein using MMP-9 ELISA kit (DMP900, R&D Systems, Minneapolis, MN, USA), and NSE protein using NSE ELISA kit (DENL20, R&D Systems, Minneapolis, MN, USA). We centrifuged plasma samples at 2,500 g for 10 min at 4 °C and added protease inhibitor (Protease Inhibitor Cocktail Set I (539131, Millipore-Sigma, Burlington, MA, USA; 1:50 dilution) to the supernatant. We used undiluted samples for S100β and NSE ELISA and diluted samples 1:20 for MMP-2 ELISA and 1:40 dilution for MMP-9 ELISA. Brain tissue samples were analyzed for Aβ40, Aβ42 and tau protein levels using the human Aβ40 ELISA kit (KHB3481, Thermo Fisher Scientific, Waltham, MA, USA), human Aβ42 ELISA kit (KHB3441, Thermo Fisher Scientific, Waltham, MA, USA) and human Tau ELISA kit (ab273617, Abcam, Cambridge, MA, USA). Brain homogenates were diluted at 1:20,000 for Aβ40 ELISA, 1:5,000 for Aβ42 ELISA, and 1:4,000 for Tau ELISA. Absorbance values were measured at 450 nm using a Synergy H1 microplate reader (BioTek® Instruments, Winooski, VT, USA). Standard curves were computed using Gen5 software (version 3.08.01) with a non-linear 4-parameter-logistic curve. Brain Aβ and tau concentrations were normalized to total wet brain weight for each sample.

X-CLARITY™ brain tissue clearing

Frozen brain tissue samples were manually sectioned (1 cm length × 1 cm width × 1 mm thickness) on an acrylic coronal brain matrix (BSA6000C, Braintree Scientific, Braintree, MA, USA) and fixed for 24 h in 4% paraformaldehyde (J61899, Thermo Fisher Scientific, Waltham, MA, USA). Fixed brain sections were rinsed with HyClone™ phosphate-buffered saline (PBS, SH30256.01, Cytiva LifeSciences, Marlborough, MA,

Table 2 List of primary antibodies used for immunohistochemistry with cleared human brain tissues

Primary antibody	Vendor	Catalog #	Lot#	Dilution	Concentration[a]	Immunogen	Clonality	Isotype	Host
Glial fibrillary acidic protein (GFAP)	Cell SIGNALLING technology	3670S	#5, #7	1:100	0.1 mg/mL	Human GFAP (full-length)	Polyclonal	IgG1	Mouse
Collagen-IV (COL-IV)	Abcam	ab6586	GR3350938-5, GR3350938-10, GR3317997-3	1:100	0.1 mg/mL	Human COLIV (full-length)	Polyclonal	IgG	Rabbit
Glucose transporter-1 (GLUT-1)	Abcam	ab115730	GR3266142-3	1:100	0.158 mg/mL	Proprietary Information	Monoclonal	[EPR3915]	Rabbit
Platelet derived growth factor—beta subunit (PDGFRβ)	Novus biologicals	AF385	B1W0621031	1:20	10 µg/mL	Mouse myeloma cell line NS0-derived recombinant human PDGFRβ Leu33-Phe530 (Glu-241Asp)	Polyclonal	IgG	Goat
Von Willebrand Factor (vWF)	Abcam	ab6994	GR3349817-1	1:100	86 µg/mL	Purified vWF (full-length) from human plasma	Polyclonal	IgG	Rabbit
Fibrinogen	Agilent	A0080	41273241	1:100	57 mg/mL	Fibrinogen isolated from human plasma	Polyclonal	IgG	Rabbit
Claudin-5	Thermo fisher scientific	34-1600	XA337901	1:500	0.5 µg/mL	C-terminal region (aa 1-218) of mouse claudin-5	Polyclonal	IgG	Rabbit
Zonula occludens-1	Thermo fisher scientific	40-2300	XA337915	1:100	2.5 µg/mL	N-terminal region (aa 1-1745) of human/dog/mouse/rat ZO-1	Polyclonal	IgG	Rabbit
Vascular cell adhesion molecule-1	Abcam	ab134047	GR3415300-6	1:100	4.37 µg/mL	Proprietary Information	Monoclonal	IgG	Rabbit

[a] Final Concentration in Antibody Diluent Solution (6% Bovine Serum Albumin + 0.2% Triton™ X-100 + 0.01% Sodium Azide + DPBS)

USA; 5 × 5 min per wash) and incubated overnight at 4 °C in 0.25% initiator solution (C13104, Logos Biosystems, Annandale, VA, USA) dissolved in X-CLARITY™ hydrogel solution (C13103, Logos Biosystems, Annandale, VA, USA). After overnight incubation, sections were placed in the X-CLARITY™ system (C20001, Logos Biosystems, Annandale, VA, USA) for polymerization (3 h, − 90 kPa, 37 °C). Polymerized brain samples were rinsed with PBS (5 × 5 min per wash) and processed in the X-CLARITY™ tissue clearing system II (C30001, Logos Biosystems, Annandale, VA, USA) for 24–30 h.

Immunohistochemistry, confocal imaging, and image analysis of tissue sections

Cleared brain tissue slices were rinsed with sterile-filtered washing buffer (HyClone™ PBS, SH30256.01, Cytiva LifeSciences, Marlborough, MA, USA; 0.2% Triton™ X-100 Surfact-Amps™ Detergent Solution, 28314, Thermo Fisher Scientific, Waltham, MA, USA; 0.01% Sodium Azide, 170419, Millipore-Sigma, Burlington, MA, USA) and incubated for 7 days with primary antibody solution (Table 2). Incubated samples were rinsed with washing buffer and exposed to a secondary antibody solution for 72 h (Table 3). Samples were rinsed with washing buffer, then rinsed with PBS, and finally rinsed with deionized water (3 × 5 min per wash) and mounted in X-CLARITY™ Mounting Solution (Refractive Index: 1.46; C13101, Logos Biosystems, Annandale, VA, USA) for 3 h at room temperature prior to confocal imaging. For each sample, Z-stack images of capillary networks were acquired with a Nikon A1R laser-scanning confocal microscope (Nikon Instruments Inc., Melville, NY, USA) using the 561 nm and 638 nm laser lines and a 40 × objective (Nikon Plan Apochromat 40x; 1.15 NA; water immersion; working distance 0.59 – 0.61 mm). Z-stacks were acquired at 5 µm steps, 30–50 steps,

Table 3 List of secondary antibodies used for immunohistochemistry with cleared human brain tissues

Secondary antibody	Vendor	Catalog #	Lot #	Dilution	Concentration[a]
AlexaFluor™ 568 Donkey-anti-Mouse IgG (pre-adsorbed)	Abcam	ab175700	GR3408409-1, 1001005613	1:250	8 µg/mL
AlexaFluor™ 647 Donkey-anti-Goat IgG (pre-adsorbed)	Abcam	ab150135	GR3324428-3	1:250	8 µg/mL
AlexaFluor™ 568 Donkey-anti-Goat IgG (pre-adsorbed)	Abcam	ab150135	GR3278446-2	1:250	8 µg/mL
AlexaFluor™ 647 Donkey-anti-Rabbit IgG (pre-adsorbed)	Abcam	ab150067	GR3312455-3, GR3360128-2	1:250	8 µg/mL
AlexaFluor™ 568 Goat-anti-Rabbit IgG (pre-adsorbed)	Thermofisher scientific	A-11036	1832035	1:500	4 µg/mL

[a] Final concentration in antibody diluent solution (6% Bovine Serum Albumin + 0.2% Triton™ X-100 + 0.01% Sodium Azide + DPBS)

318.48 µm × 318.48 µm × 100 µm, 0.25–0.5 frames per second, 35.8 µm pinhole, < 5% laser power, 100 master gain, 0 or -10 digital offset. Acquired Z-stacks were processed using the 'Stacks—Z Project—Maximum Intensity' plugin in Fiji/ImageJ (v.1.53 g, Wayne Rasband, NIH, USA) to obtain maximum intensity projection (MIP) images (20 steps, 5 µm step size). Mean intensities of MIPs were measured using the 'Analyze—Measure' Fiji/ImageJ plugin. Vessel diameters were measured manually using the 'Straight Line' tool. Since reactive astrogliosis is a common pathological change in AD brain tissue Sects. [35–37], we cleared brain tissue sections using the X-CLARITY™ tissue-clearing method, followed by immunostaining and confocal microscopy to identify the extent of glial fibrillary acidic protein (GFAP) immunoreactivity in brain tissue slices [38, 39].

Human brain capillary isolation

Capillaries were isolated from human cortex tissue using our established protocol [16, 20, 40–46]. All reagents and consumables were purchased from Millipore-Sigma, Burlington, MA, USA. Briefly, snap-frozen brain tissue samples were thawed on ice and weighed; meninges were removed using forceps. Brain tissue was minced with a scalpel and homogenized in cold isolation buffer (Dulbecco's phosphate-buffered saline; 2.7 mM KCl, 1.47 mM KH_2PO_4, 136.9 mM NaCl, 8.1 mM, Na_2HPO_4, 0.9 mM $CaCl_2$, 0.49 mM $MgCl_2$; pH adjusted to 7.4) using a 1:3 ratio (wt/vol) of tissue/isolation buffer. Brain tissue was homogenized using a Potter–Elvehjem tissue grinder (clearance: 101–152 µm; 100 strokes at 50 rpm, 25 strokes at 75 rpm, 25 strokes at 100 rpm) followed by 30 strokes in a hand-held Dounce homogenizer (clearance: 75-127 µm). Brain homogenate was mixed with 30% Ficoll® PM400 (1:5 ratio) and centrifuged at 5800 g for 15 min at 4 °C. After centrifugation, capillary pellets were resuspended in isolation buffer containing 1% bovine serum albumin (BSA) and filtered through a 300 µm mesh followed by three 30 µm cell strain filters. Cell strainers were washed twice with 50 mL isolation buffer containing 1% BSA, and the filtered solution was centrifuged at 1500 g for 3 min at 4 °C. Isolated human brain capillaries were used for immunohistochemistry or frozen until further analysis.

Immunohistochemistry, confocal imaging, and image analysis of isolated capillaries

Isolated human brain capillaries were incubated overnight at 4 °C with primary antibodies against claudin-5, ZO-1, or VCAM-1 (Table 2) in glass bottom dishes (KIT-5030B, WillCo-dish®, Electron Microscopy Sciences, Hatfield, PA, USA). Capillaries were rinsed with PBS containing 1% BSA, incubated with secondary antibody against rabbit IgG (Table 3) for 1 h at room temperature, and stained with DAPI (S9980, Selleckchem, Houston, TX, USA; 1:1000 dilution; 10 µg/mL). Immunostained capillaries were imaged with a Nikon A1R laser-scanning confocal microscope (Nikon Instruments Inc., Melville, NY, USA) using the 405 nm laser line (100% laser power, 130 master gain, 0 digital offset) and the 561 nm laser line (5% laser power, 40 master gain, 0 digital offset [44, 46]. Images were acquired using a 40 × objective (Nikon Plan Apochromat 40x; 1.15 NA; water immersion; working distance 0.59–0.61 mm) and 4 × NiQuist Zoom (79.62 µm × 79.62 µm, 30.65 µm pinhole, 0.25 frames per second). Confocal images were split into individual channels for fluorescence intensity analysis, and mean intensities were retrieved from 3 regions of interest along the capillary membranes.

Human brain lysate and human capillary lysate extraction

Human brain tissue and isolated human brain capillaries were lysed in 200 µL lysis buffer (CelLytic™ MT Cell Lysis Reagent, C3228, Millipore-Sigma, Burlington, MA, USA) containing 5X cOmplete™ protease inhibitor cocktail (11697498001, Millipore-Sigma, Burlington, MA, USA). Lysed tissue samples were homogenized using an ultraspeed polytron homogenizer (PT 2500 E stand dispersing device + PT-DA 3 mm dispersing generator, Kinematica Inc., Bohemia, NY, USA; 30,000 rpm, 3 min 20 s). Homogenates were centrifuged at 30,000 rpm for 30 min at 4 °C in a TLA100.3 fixed-angle rotor using a Beckman Coulter Optima TLX Ultracentrifuge (359732; Beckman Coulter, Brea, CA, USA) to collect brain lysate and

capillary lysate (supernatant). Supernatants were frozen at − 20 °C until further analysis. Protein concentrations for brain and capillary lysate samples were determined by Bradford protein assay [47].

JESS™ electrophoresis

All reagents listed below, except primary antibodies, were purchased from ProteinSimple/Bio-Techne (Minneapolis, MN, USA). Samples were diluted in 5 × Fluorescent Master Mix and 0.1 × Sample Buffer to a final concentration of 0.05 mg/mL. Diluted samples were vortexed, centrifuged, and denatured for 10 min at 70 °C. Samples were probed using rabbit-anti-claudin-5 antibody (34-1600, ThermoFisher Scientific, Waltham, MA, USA; 1:50 dilution or 5 µg/mL) and mouse-anti-β-actin antibody (CST3700, Cell Signaling Technology, Danvers, MA, USA; 1:50 dilution or 6.24 µg/mL) in a duplex assay. Loaded plates were centrifuged at 1000 g for 5 min at 4 °C and assayed over 3 h by chemiluminescence. Data was annotated and analyzed using Compass software for SW (version 6.2.0). The peak area for claudin-5 was normalized by corresponding values for β-actin to compare protein concentration across samples [41, 48, 49].

Statistical analysis

Simple comparisons between AD and CNI were performed using Prism (v8.4.0; GraphPad, San Diego, CA, USA). Data were tested for Gaussian distributions via Shapiro–Wilk test and QQ plots. Normally distributed datasets were tested using the Student's unpaired (two-tailed) *t*-test with Welch's correction. Non-normally distributed datasets were tested using the Mann–Whitney rank sum test. All other analyses were carried out with R statistical software [50]. Pearson, polychoric, or polyserial correlations, as appropriate, were estimated for multiple outcomes [51], and *p* values were adjusted for multiple comparisons by Benjamini-Hochberg (BH fdr) false discovery rate [52]. Microvascular diameters were compared to AD diagnosis, Braak staging, CA, CAA severity score, neuritic NP burden, CDR score, MMSE score, apolipoprotein E (APOE) genotype, sex, education, and brain Aβ levels (predictor variables) by generalized linear mixed-level modeling with the "lme4" package, v. 1.1–34 [53]. Age was controlled via case-matching in the sample selection process. The following characteristics were considered random factors for analysis: reference ID, laser line, HV gain, zoom, scan speed, offset, sample collection dates, antibody concentrations, and lot numbers. Potential random effects with an estimated standard deviation of less than 10^{-4} were excluded as being of too small effect. Marginal coefficients of determination (R^2) were calculated to quantify variations for generalized linear mixed-level models [54]. Plasma-based biomarkers (S100β, NSE, MMP-2, MMP-9) were modeled as predictors for AD diagnosis, Braak staging, CA, CAA severity score, neuritic NP frequency, CDR score, MMSE score, Aβ40 and Aβ42 brain levels, and brain tau levels (response). Association with the AD case group was modeled by logistic regression. Association for individual Braak stages, CA, CAA, neuritic NP frequency, and CDR were modeled by ordinal logistic regression, using the "ordinal" package v. 2022.11-16 [55], proportional odds assumption was tested by likelihood ratio testing vs. models that coded each predictor as "nominal", with non-significant difference taken to mean non-violation of the assumption [55]. MMSE scores, brain Aβ42 levels, brain Aβ40 levels, and brain tau were modeled by generalized linear modeling. Models for each biomarker vs. each predictor were evaluated based on the lowest second-order Akaike Information Criterion with a correction for small sample sizes (AICc; [56]). AICc is a measure of entropy (information lost) with lower AICc indicating less information lost in the model compared to competing models of the same response data. Samples with missing data points, specifically, one subject lacked DP, NP, and NFT scores, and a second subject did have measurements of tau or claudin 5 proteins, were excluded from analyses. Model selection was followed by analysis of variance, commonly called "ANOVA"; *p* values were adjusted for multiple comparisons by BH fdr. We evaluated goodness of fit for ordinal models with Nagelkerke's R^2 [57], used Tjur's *D* [58] for logistic models, and used ω^2 for GLMs [58, 59]. We further estimated the optimal sample size from power calculations from R^2 or *D*.

Results

We previously demonstrated that Aβ drives barrier dysfunction and that Aβ accumulation in the form of CAA contributes to injuries of the neurovasculature, leading to a dysfunctional barrier [16, 20, 44–46]. Based on these previous findings, the objective of our study was to assess markers for blood–brain barrier dysfunction in postmortem tissue samples from CNI and AD patients and determine whether these markers are associated with AD pathology and cognitive impairment against a background of CAA.

Participants

Among the 19 included UK-ADRC participants, 9 were CNI and 10 were clinically diagnosed with AD-type dementia and had a neuropathological diagnosis of AD (Table 1; Fig. 1). The CNI group was older at death (86.7 vs 82.2 y), more likely to be male (5:4 vs. 3:7) and had higher educational attainment (16 vs 14 y). Among the AD group, 9/10 had Braak NFT Stage of VI with one at Stage V. Among the CNI group, all

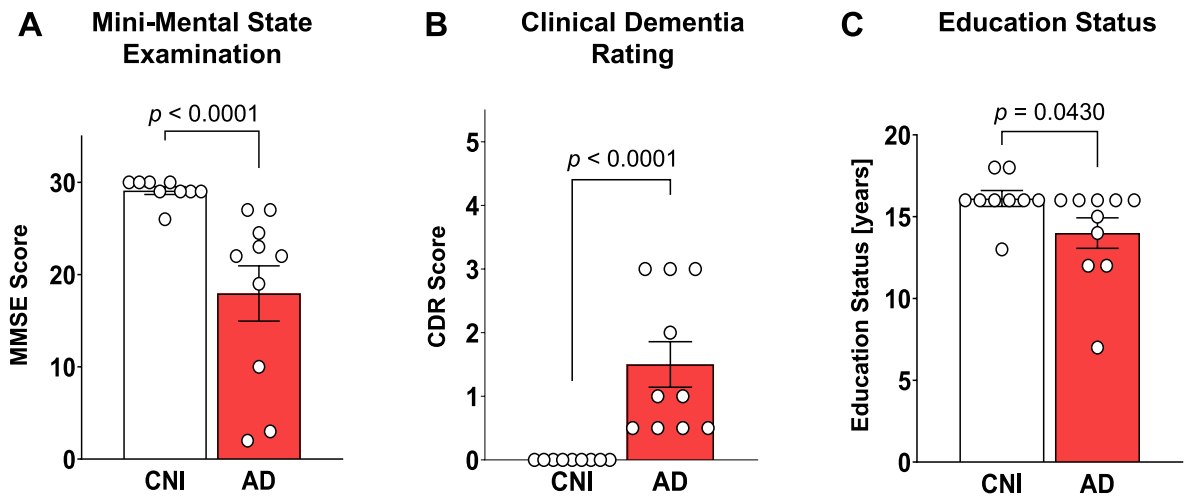

Fig. 1 Cognitive Status of CNI and AD Patients. **A** MMSE scores in AD patients were 1.6-fold lower than in CNI ($p < 0.0001$). **B** Clinical Dementia Rating was 1.5 for AD patients and zero for CNI ($p < 0.0001$). **C** Education attainment in AD patients was 2 years less than in CNI ($p = 0.043$). *p* values were estimated by Mann–Whitney Rank-Sum test

Braak NFT Stages were III or lower. CAA was Mild (5/9), Moderate (2/9) or Severe (1/9) in the CNI group, and Mild (4/10), Moderate (2/10) or Severe (4/10) in the AD group. CAA scores were severe in cases with one or two APOE ε4 alleles, regardless of cognitive group (Table 4).

Table 4 Associations between patient characteristics, neuropathological, cognitive, and biochemical outcomes of CNI and AD patients.

	Braak Stage	Cortical Atrophy (CA) Score	CAA Score	NP Score	NFT Score	CDR Score	Brain Aβ42 Level	Brain Aβ40 Level	Brain Tau Level	Claudin-5/β-actin Peak Area Ratio	*APOE* ε Genotype	Sex	Plasma S100B Level	Plasma NSE Level	Plasma MMP2 Level	PlasmaMMP9 Level
Braak Stage		***0.577***	0.339	***0.650***	***0.502***	***0.597***	***0.662***	0.375	***0.444***	-0.150	0.140	0.275	***0.908***	***-0.661***	***-0.655***	***0.540***
Cortical Atrophy (CA) Score	***0.577***		-0.049	0.237	0.250	***0.543***	***0.622***	0.124	0.213	***-0.565***	-0.201	-0.283	0.409	-0.099	-0.389	0.143
CAA Score	0.339	-0.049		0.137	0.167	-0.072	0.244	0.298	***0.598***	-0.253	***0.536***	***0.481***	0.101	-0.095	0.085	-0.073
NP Score	***0.650***	0.237	0.137		***0.525***	0.374	***0.585***	***0.506***	0.320	-0.058	-0.154	0.270	***0.715***	***-0.538***	***-0.536***	0.364
NFT Score	***0.502***	0.250	0.167	***0.525***		***0.489***	0.242	***0.417***	0.082	-0.091	0.026	0.236	0.215	0.141	-0.085	0.116
CDR Score	***0.597***	***0.543***	-0.072	0.374	***0.489***		***0.575***	0.103	0.042	-0.313	0.077	-0.105	0.384	-0.052	***-0.704***	0.311
Brain Aβ42 Level	***0.662***	***0.622***	0.244	***0.585***	0.242	***0.575***		0.274	0.221	***-0.407***	-0.098	0.150	***0.655***	-0.361	***-0.600***	0.333
Brain Aβ40 Level	0.375	0.124	0.298	***0.506***	***0.417***	0.103	0.274		***0.601***	-0.203	0.138	0.080	***0.569***	-0.238	-0.059	0.398
Brain Tau Level	***0.444***	0.213	***0.598***	0.320	0.082	0.042	0.221	***0.601***		-0.340	0.114	0.102	0.298	-0.186	0.071	0.208
Claudin-5/β-actin Peak Area Ratio	-0.150	***-0.565***	-0.253	-0.058	-0.091	-0.313	***-0.407***	-0.203	-0.340		0.019	0.359	0.033	-0.165	0.095	0.224
***APOE* ε Genotype**	0.140	-0.201	***0.536***	-0.154	0.026	0.077	-0.098	0.138	0.114	0.019		0.271	0.189	-0.035	-0.099	-0.169
Sex	0.275	-0.283	***0.481***	0.270	0.236	-0.105	0.150	0.080	0.102	0.359	0.271		0.143	-0.163	0.143	-0.035
Plasma S100B Level	***0.908***	0.409	0.101	***0.715***	0.215	0.384	***0.655***	***0.569***	0.298	0.033	0.189	0.143		***-0.774***	***-0.697***	0.339
Plasma NSE Level	***-0.661***	-0.099	-0.095	***-0.538***	0.141	-0.052	-0.361	-0.238	-0.186	-0.165	-0.035	-0.163	***-0.774***		***0.495***	-0.329
Plasma MMP2 Level	***-0.655***	-0.389	0.085	***-0.536***	-0.085	***-0.704***	***-0.600***	-0.059	0.071	0.095	-0.099	0.143	***-0.697***	***0.495***		-0.083
Plasma MMP9 Level	***0.540***	0.143	-0.073	0.364	0.116	0.311	0.333	0.398	0.208	0.224	-0.169	-0.035	0.339	-0.329	-0.083	

Boldface shows significant coefficients ($p < 0.05$), adjusted (BH fdr) for 120 simultaneous correlations. Blank cells indicate correlation coefficients not calculated due to like-to-like comparison.

Aβ pathology

We determined Aβ pathology in CNI and AD brain tissue samples by histological staining, immunohistochemistry, and ELISA. First, we stained postmortem brain tissue sections for Aβ plaques using modified Bielschowsky silver staining [24–28]. To assess the severity of frontal Aβ plaque pathology, we classified plaques as diffuse Aβ plaques (DPs) or neuritic Aβ plaques (NPs). Plaque quantification showed a 2.4-fold higher DP count ($p=0.003$) in AD brain tissue Sects. (44 ± 3 counts/mm^2) compared to CNI brain tissue Sects. (18 ± 6 counts/mm^2; Fig. 2A). Likewise, the number of NPs in AD brain tissue Sects. (16 ± 3 counts/mm^2) was 2.3-fold higher ($p=0.039$) compared to CNI brain tissue Sects. (7 ± 3 counts/mm^2; Fig. 2B). We also quantified neuritic plaque frequency in brain tissue samples. NP counts were similar for both CNI and AD patients (CNI: 1.2 ± 0.2; AD: 1.2 ± 0.2; Fig. 2C). We then assessed the severity of CAA pathology and found that CAA pathology in AD brain tissue Sects. (4 mild, 2 moderate, 4 severe) was more frequent and severe when compared with CAA pathology in CNI brain tissue Sects. (5 mild, 3 moderate, 1 severe; Fig. 2D). Next, we quantified Aβ40 and Aβ42 levels in brain tissue samples by ELISA and found that brain Aβ40 levels in samples from AD patients (12.9 ± 4.6 ng/mg) were 4.2-fold higher ($p=0.022$) compared to levels in samples

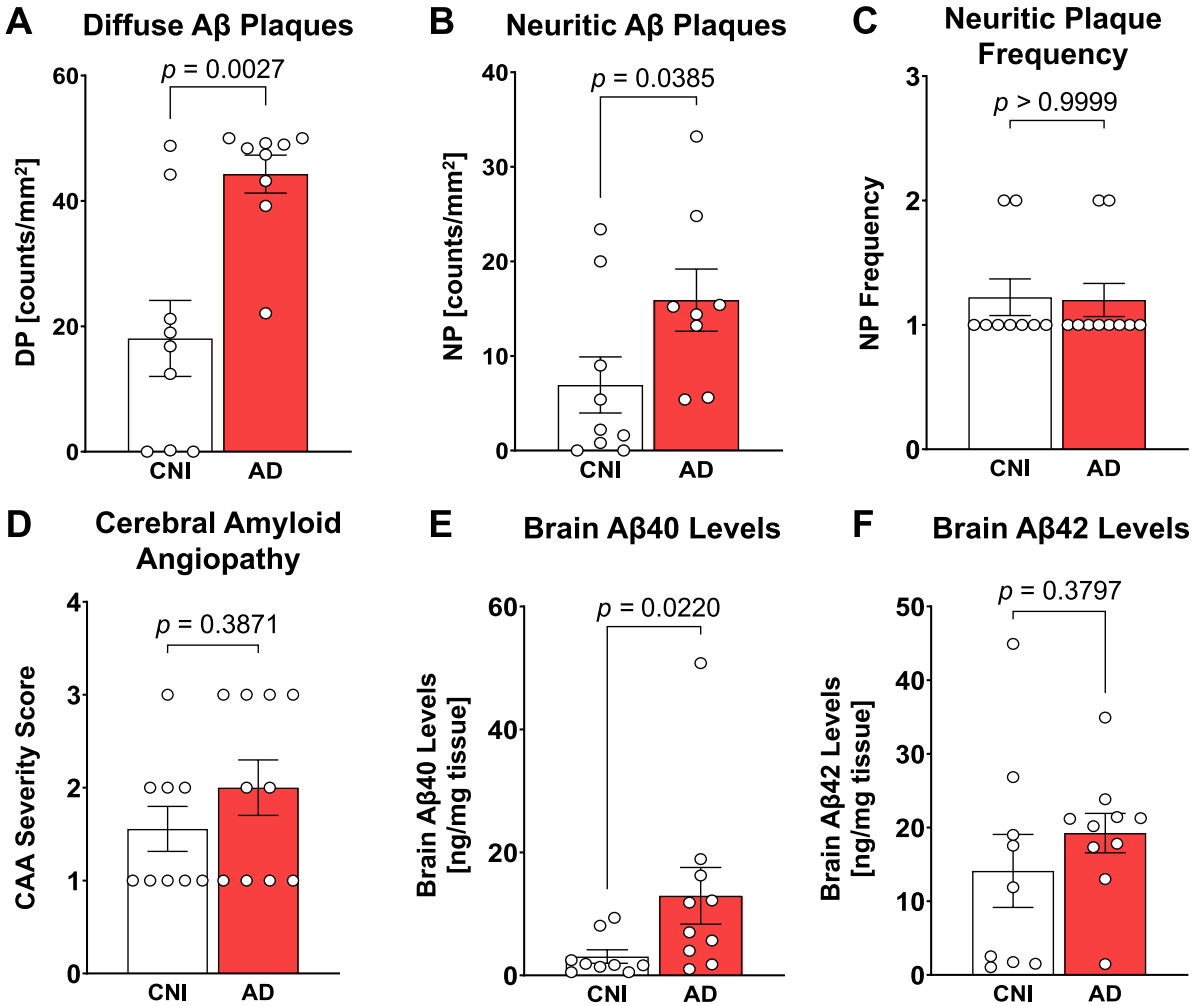

Fig. 2 Aβ Pathology in Brain Samples from CNI and AD Patients. **A** Diffuse Aβ plaques in AD patients were 2.5-fold higher ($p=0.003$) compared to diffuse Aβ plaques in CNI. **B** Neuritic Aβ plaques in AD patients were 2.3-fold higher ($p=0.039$) than neuritic Aβ plaques in CNI. **C** Neuritic plaque frequency was similar for AD and CNI patients ($p=1.000$). **D** CAA instances were more frequent and severe in AD patients (4 severe cases, 2 moderate cases, 3 mild cases) when compared with CAA instances in CNI (1 severe case, 3 moderate cases, 5 mild cases). **E** Brain Aβ40 levels in AD brain samples were 4.3-fold higher ($p=0.022$) than in CNI brain samples. **F** Brain Aβ42 levels in AD brain samples were similar ($p=0.380$) to those in CNI brain samples. *p* values were estimated by Mann–Whitney Rank-Sum test in (**A**–**E**) and by Student's t-test with Welch's correction in (**F**)

from CNI (3.1 ± 1.1 ng/mg; Fig. 2E). Note that brain Aβ40 levels were higher in patients with consensus AD diagnosis (r = 0.851) and in patients with severe CAA pathology (r = 0.880; Table 4). Aβ42 levels in brain tissue samples from AD patients (19.2 ± 2.7 ng/mg) were 1.4-fold higher ($p = 0.380$) compared to levels in samples from CNI (14.1 ± 5.0 ng/mg; Fig. 2F). Together, our findings show increased Aβ brain levels, elevated plaque counts, and more frequent instances of severe CAA in brain tissue samples from AD patients compared to those found in samples from CNI, indicating that our sample is typical of what is expected of the differences between AD and CNI.

Tau pathology

Next, we assessed tau pathology in brain tissue samples from CNI and AD patients by determining Braak stages and measuring NFTs and total tau levels. We compared Braak stages vs. diagnosis with ordinal logistic regression and found that the frequencies of Braak scores separated distinctly by CNI vs. AD. Specifically, stages I, II, and III were unique to CNI, while stages V and VI were only found in AD subjects (Fig. 3A). Braak staging was also associated with increased brain Aβ40 levels (r = 0.878; Table 4), which suggests some degree of association between the two drivers of AD. NFT scores in AD brain tissue Sects. (16.8 ± 5.9 counts/mm^2) were 168-fold higher ($p < 0.001$) than in CNI brain tissue Sects. (0.1 ± 0.1 counts/mm^2; Fig. 3B). ELISA findings revealed similar tau protein levels in brain tissue samples from CNI (23.3 ± 3.2 ng/mg) and AD patients (20.3 ± 4.2 ng/mg; Fig. 3C). Overall brain tissue samples from AD patients had elevated tau pathology compared to samples from CNI.

Structural changes

We determined structural changes based on cortical atrophy and astrogliosis. Cortical atrophy is determined by postmortem examination of brain tissue and rated on a severity scale of 0–3. Cortical atrophy scores in AD patients (5 mild and 4 moderate cases; average rating: 1.3 ± 0.2) were about fourfold higher ($p = 0.006$) than cortical atrophy scores in CNI (9 cases with no atrophy, 1 mild, 1 moderate, average rating: 0.3 ± 0.2; Fig. 4A). Correlation analysis showed that cortical atrophy scores were associated with a consensus AD diagnosis (r = 0.710), NFT scores (r = 0.692), and gender (r = 0.852; Table 4). GFAP immunoreactivity was similar in CNI and AD brain tissue slices (CNI: 27.7 ± 4.0 billion a.u./mm^2; AD: 35.6 ± 4.0 billion a.u./mm^2; Fig. 4B). Generalized linear mixed-level modeling showed that GFAP immunoreactivity was not associated with patient characteristics (Table S1, Fig. S1). AD brain tissue sections have extensive cortical atrophy but similar GFAP immunoreactivity in the analyzed regions of interest when compared with CNI brain tissue sections. We detected a significant elevation (110 ± 11 vs. 72 ± 3 pg/mg total protein, $p = 0.001$) in Iba-1 levels in brain lysates from AD patients vs CNI subjects. However, we found no difference ($p = 0.911$) in levels of the transcytosis marker Caveolin-1 between CNI (11.3 ± 0.6 ng/mg) and AD (11.4 ± 0.3 ng/mg).

Microvascular diameter analysis

We used immunostained cleared brain tissue sections to visualize microvessels and measure microvascular

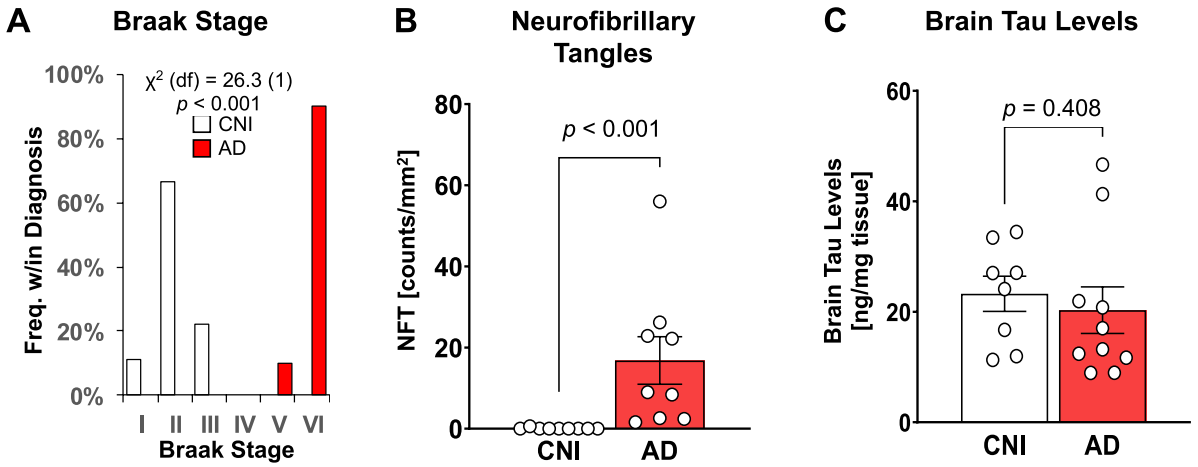

Fig. 3 Tau Pathology in Brain Samples from CNI and AD Patients. **A** Braak stages in CNI (I-III) correspond to CNI diagnosis, whereas Braak stages V and VI correspond to AD patients. **B** Neurofibrillary tangles (NFTs) in AD patients were 168-fold higher ($p < 0.001$) than those in CNI. **C** Brain tau levels were similar in CNI and AD brain tissue homogenate ($p = 0.408$). *p* values were estimated by Mann–Whitney Rank-Sum test

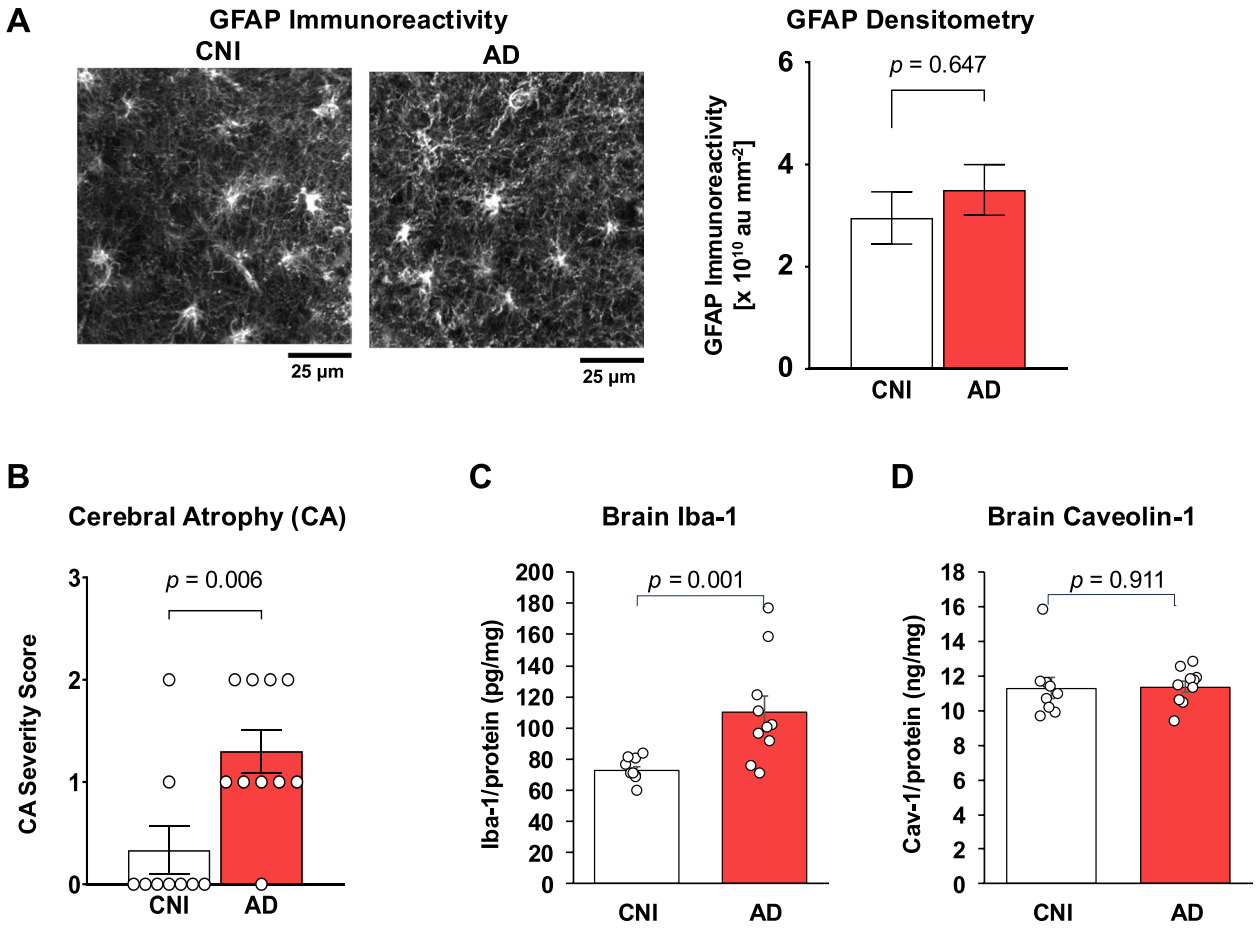

Fig. 4 Structural Changes in Brain Samples from CNI and AD Patients. **A** Cortical atrophy in AD patients was fourfold higher ($p=0.006$) than in CNI. **B** Representative confocal images of GFAP immunoreactivity in cleared AD and CNI brain tissue slices. Average GFAP immunoreactivity was similar in AD patients and CNI ($p=0.647$). *p* values estimated by Mann–Whitney Rank-Sum test. Scale Bar: 25 µm. **C** ELISA of Iba-1 showed significant ($p=0.001$) elevation in brain extract Iba-1 levels in AD compared to CNI. **D** ELISA of Caveolin-1 showed no differences in brain extract levels for CNI vs AD

diameters (Fig. 5). We used antibodies specific to five different vascular proteins: (1) collagen-IV (COL-IV), (2) platelet-derived growth factor receptor-β subunit (PDGFRβ), (3) von Willebrand factor (vWF), (4) glucose transporter-1 (GLUT-1), and (5) fibrinogen. We measured microvascular diameters for 300–600 capillaries per sample per marker. Figures 5A–E show representative confocal images of stained capillaries for each marker. We found that the mean vascular diameter for COL-IV-immunostained microvessels was 6.5 ± 0.7 µm in AD brain tissue sections and 7.3 ± 0.8 µm in CNI brain tissue sections ($p=0.121$; Fig. 5A). Mean vascular diameters for PDGFRβ-immunostained microvessels were 6.5 ± 0.6 µm for AD samples and 6.6 ± 0.9 µm for CNI samples ($p=0.987$; Fig. 5B). Microvascular PDGFRβ diameters showed no significant associations with any of the candidate predictors in this study (Table S2). For vWF-immunostained microvessels, mean diameters were 5.9 ± 0.6 µm for AD brain tissue sections and 6.1 ± 0.6 µm for CNI sections ($p=0.464$; Fig. 5C). For GLUT-1-immunostained microvessels, mean diameters were 5.1 ± 0.5 µm for AD brain tissue sections and 5.2 ± 0.6 µm for CNI sections ($p=0.811$; Fig. 5D). Mean vessel diameters for fibrinogen-labeled sections were 4.7 ± 0.7 µm for AD brain sections and 4.0 ± 0.5 µm for CNI sections ($p=0.298$; Fig. 5E). Generalized linear mixed-level modeling showed that microvascular COL-IV diameters tended to decrease non-linearly with higher Braak stages (Fig. 6A, Table 5), increased NP scores (Fig. 6B; Table 5), and increased brain Aβ40 levels (Fig. 6C; Table 5). These associations suggest a thinning of the basement membrane in brain tissue from AD patients. Fibrinogen diameters were higher in patients with Braak stages I, III, and VI compared to those at Braak stages II and V (Fig. 6D,

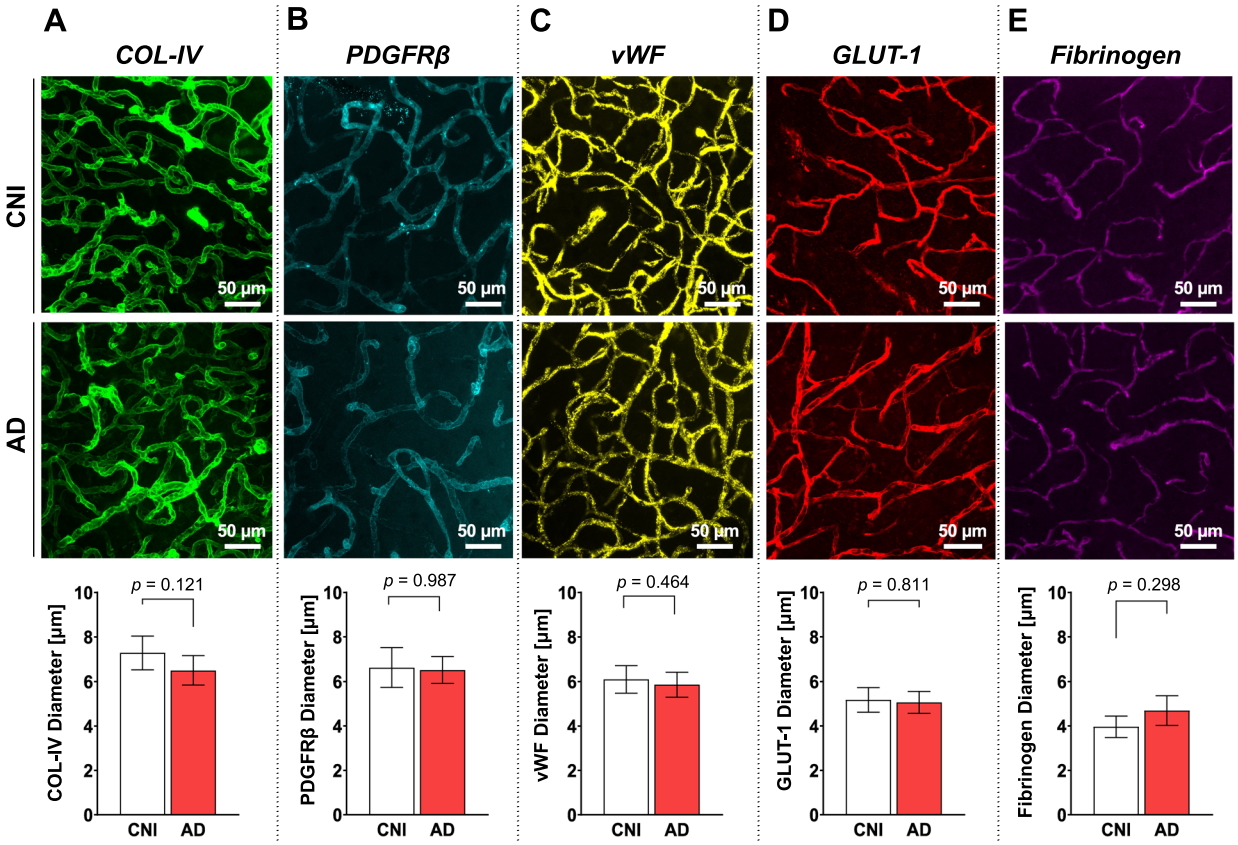

Fig. 5 Microvascular Diameter Analysis of Cleared Brain Tissue Sections. **A**–**E** Representative images and average vascular diameters from immunostained brain tissue sections. We used antibodies against **A** COL-IV, **B** PDGFRβ, **C** vWF, **D** GLUT-1, and **E** fibrinogen to visualize the vasculature and measure vascular diameters. Graphical plots of mean vascular diameters accompany representative images. Scale Bar: 50 µm. $p = 0.121$ (COL-IV), $p = 0.987$ (PDGFRβ), $p = 0.464$ (vWF), $p = 0.811$ (GLUT-1), $p = 0.298$ (fibrinogen)

Table 5). Fibrinogen diameters were smaller in brain tissues with higher NP frequency (Fig. 6E, Table 5). No other predictor-response combinations showed significant associations (Table S2-S6, Fig. S2-S6). Thus, diameter analysis revealed that AD pathology correlates with thinner COL-IV diameters and increased fibrinogen diameters.

Tight junction protein expression

We assessed protein expression of claudin-5, zonula occludens-1 (ZO-1), and vascular cell adhesion molecule-1 (VCAM-1) in brain capillaries isolated from AD and CNI brain tissue samples by immunostaining (Fig. 7). We analyzed the mean fluorescence intensities across the capillary endothelial cell membranes and found that claudin-5 immunofluorescence was 971 ± 129 a.u. in capillaries from AD patients and 1144 ± 208 a.u. in capillaries from CNI ($p = 0.643$; Fig. 7A). Mean fluorescence intensity for ZO-1 was 1018 ± 163 a.u. in capillaries isolated from AD tissue samples and 859 ± 77 a.u. for capillaries from CNI ($p = 0.755$; Fig. 7B). Mean VCAM-1 fluorescence intensity was 924 ± 83 a.u. for CNI capillaries and 815 ± 96 a.u. for capillaries from AD ($p = 0.363$; Fig. 7C).

We used the Simple Western™ JESS capillary electrophoresis assay to quantify claudin-5 protein levels in 12 out of 19 brain tissue samples (Fig. 8A). Seven samples were excluded from this assay due to limited tissue amounts. To account for variations in band intensity, we calculated the claudin-5/β-actin peak area ratio. Pairwise comparison of claudin-5/β-actin peak area ratio (Fig. 8B) indicated that, for CNI samples, claudin-5/β-actin peak area ratios varied from 0.4 to 5.9 with an average peak area ratio of 2.1 ± 0.9, and, for AD samples, claudin-5/β-actin peak area ratios varied from 0.5 to 9.3 with an average peak area ratio of 2.5 ± 1.4. Claudin-5/β-actin peak area ratios were not significantly different between CNI and AD capillary lysate samples ($p = 0.937$). Correlation analysis showed that claudin-5/β-actin peak areas were associated with cortical atrophy ($r = -0.673$), APOE ε4 genotype ($r = 0.704$), and gender ($r = -0.821$; Table 4). Overall, claudin-5 protein levels did not significantly

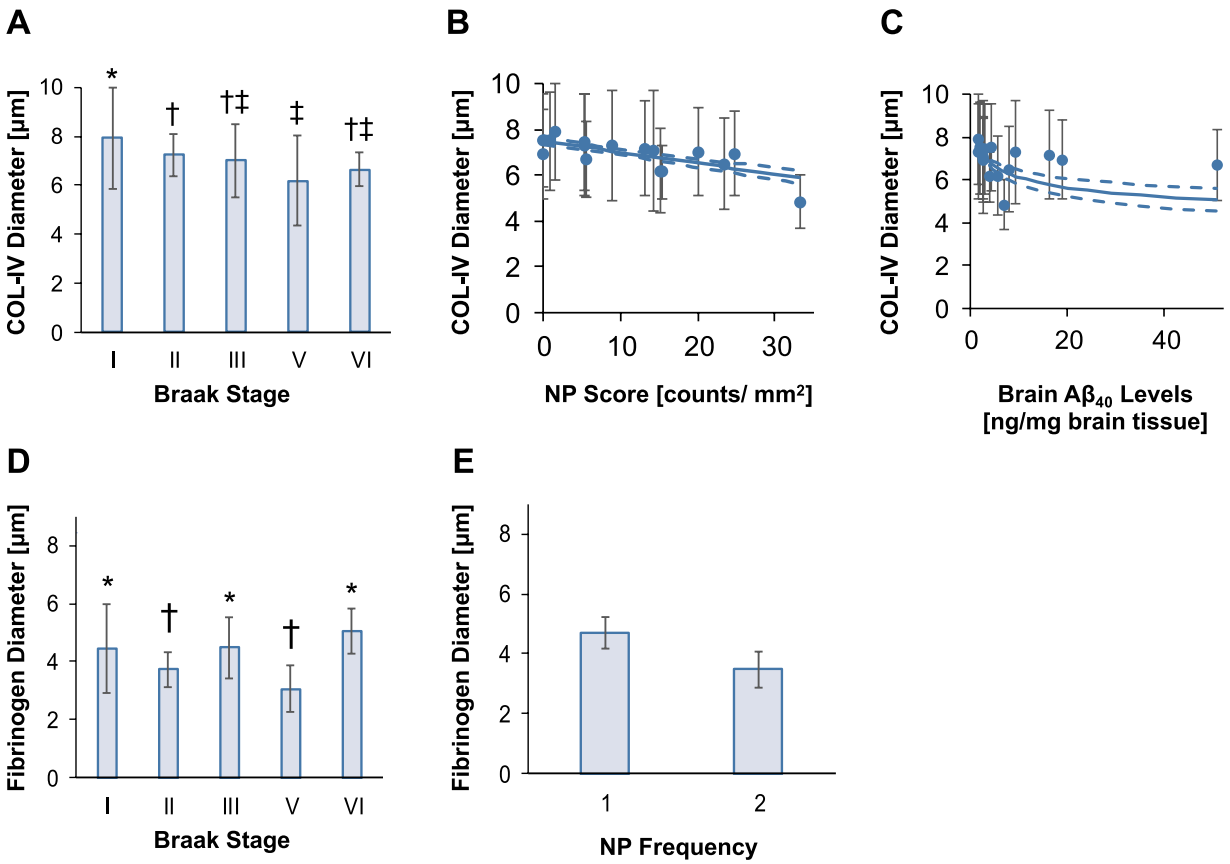

Fig. 6 Associations between Microvascular Diameters and Pathological Outcomes. **A** Microvascular COL-IV diameters at different Braak stages. **B** Microvascular COL-IV diameters decrease with increasing NP scores. **C** Microvascular COL-IV diameters versus brain Aβ40 levels. **D** Microvascular fibrinogen diameters at different Braak stages. **E** Microvascular fibrinogen diameters at different NP frequencies. Samples that do not share the same symbols in **A** and **D** are significantly different. Error bars show the standard error of the mean (SEM). Solid lines show model-predicted values and dashed lines show standard errors of model-predicted values

Table 5 Variations in microvascular diameters with neuropathological, cognitive, and biochemical predictors for CNI and AD Patients

Response	Predictor	χ^2	Raw *p* value	Adjusted *p* value[a]	R^2
COL-IV diameter (µm)	Braak stage	43.082 (4)	< 0.001	< 0.001	0.041
COL-IV diameter (µm)	NP scores	11.108 (1)	< 0.001	0.005	0.057
COL-IV diameter (µm)	Brain $A\beta_{40}$ levels (ng/mg brain tissue)	13.353 (1)	< 0.001	0.002	0.107
Fibrinogen diameter (µm)	Braak stage	26.669 (4)	< 0.001	< 0.001	0.111
Fibrinogen diameter (µm)	Neuritic plaque frequency	7.600 (1)	0.006	0.042	0.044
vWF diameter (µm)	CAA severity score	11.202 (2)	0.004	0.031	0.041
vWF diameter (µm)	Brain $A\beta_{40}$ levels (ng/mg brain tissue)	9.274 (1)	0.002	0.031	0.028

[a] Adjusted by Benjamni-Hochberg FDR

change along capillaries isolated from CNI and AD brain tissues.

Peripheral biomarker analysis

We quantified NSE, MMP-2, MMP-9, and S100β plasma levels via ELISA. In CNI samples, plasma NSE levels varied from 9.4 ng/mL to 17.2 ng/mL, with average plasma NSE levels at 12.7 ± 1.4 pg/mL (Fig. 9A). In AD samples, plasma NSE levels varied from 2.7 ng/mL to 11.0 ng/mL with average plasma NSE levels at 6.3 ± 1.0 ng/mL. Plasma NSE levels in AD patients were twofold lower than those in CNI ($p = 0.007$). In CNI, plasma MMP-2 levels varied from 235.3 ng/mL to 264.4 ng/mL with an average plasma MMP-2 concentration of 247.2 ± 5.3 ng/

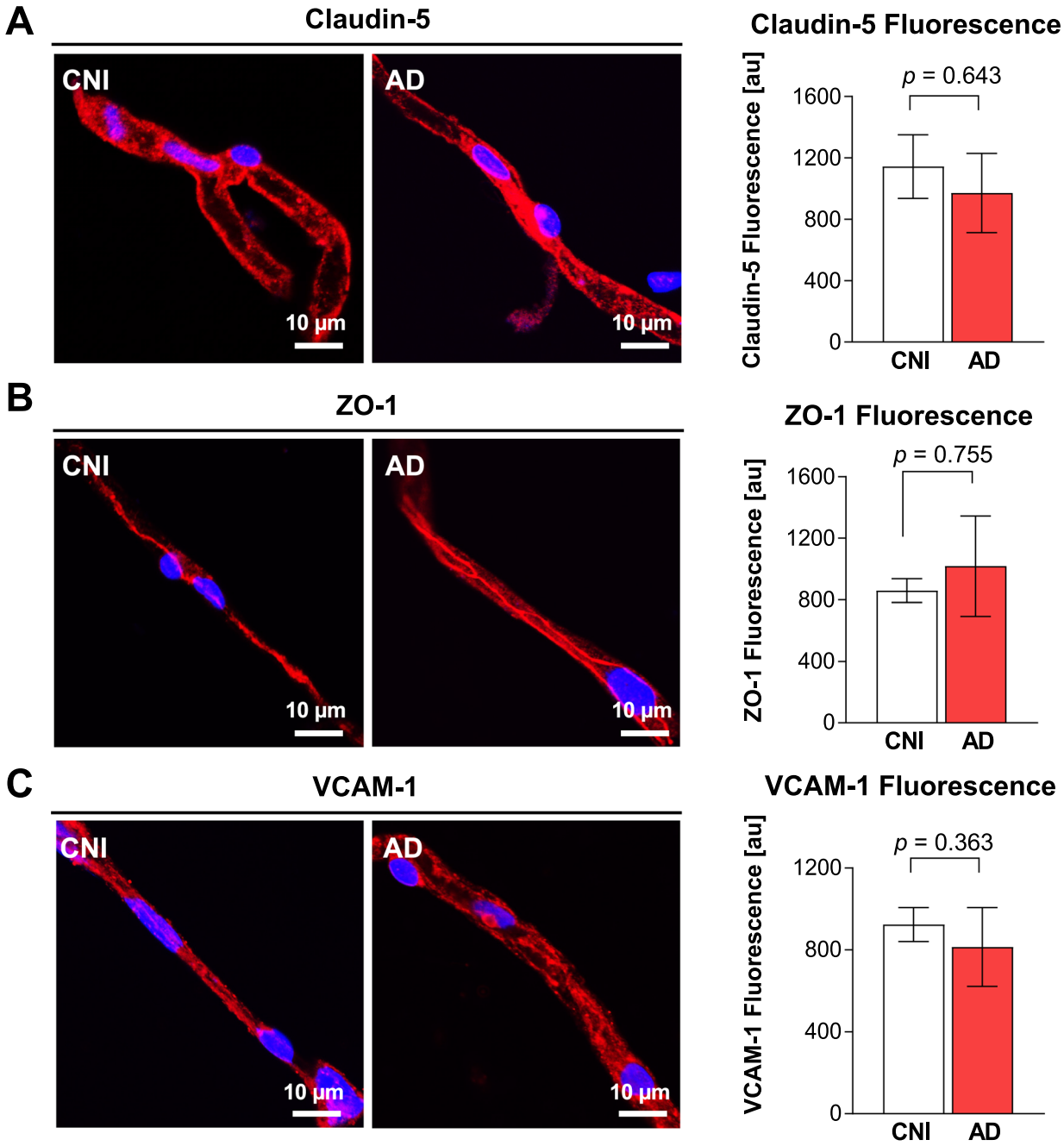

Fig. 7 Tight-Junction Protein Expression Along Isolated Microvessels. **A** Representative confocal images of claudin-5 immunoreactivity along capillaries isolated from brain tissue of AD patients and CNI. **B** Representative confocal images of ZO-1 immunoreactivity along capillaries isolated from brain tissue of AD patients and CNI. **C** Representative confocal images of ZO-1 immunoreactivity along capillaries isolated from brain tissue of AD patients and CNI. Mean intensity levels along capillary membranes are shown next to representative confocal images. AD-vs-CNI comparisons are indicated with corresponding *p* values. $p = 0.643$ (claudin-5), $p = 0.755$ (ZO-1), $p = 0.363$ (VCAM-1). Scale Bar: 10 µm

mL (Fig. 9B). In AD patients, plasma MMP-2 levels varied from 179.4 ng/mL to 237.2 ng/mL with an average plasma MMP-2 concentration of 212.3 ± 7.5 ng/mL ($p = 0.003$; 1.2-fold difference). Plasma MMP-9 levels for CNI samples varied from 61.5 ng/mL to 94.1 ng/mL with average plasma MMP-9 levels at 71.5 ± 5.8 ng/mL (Fig. 9C). In contrast, plasma MMP-9 levels for AD samples varied from 25.5 ng/mL to 400.0 ng/mL with average

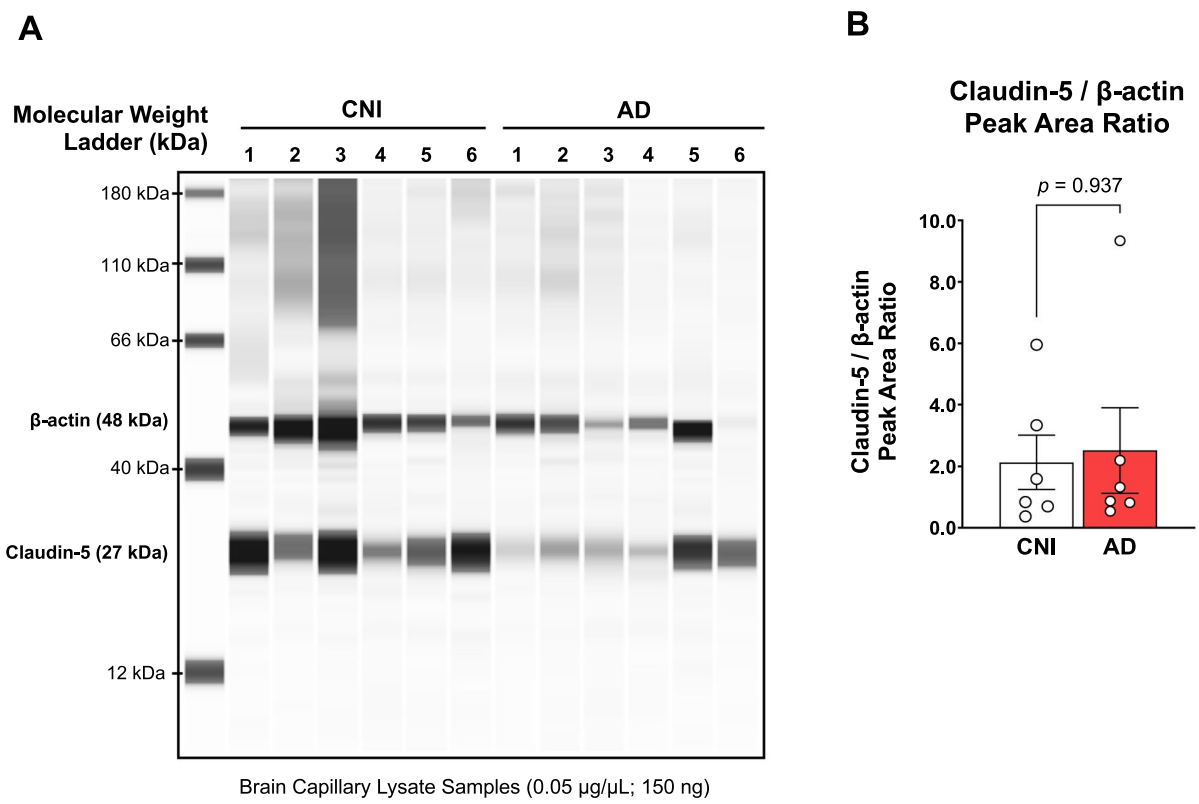

Fig. 8 Claudin-5 Protein Levels in Brain Capillary Lysate Samples. **A** JESS™ capillary electrophoresis pictograph showing claudin-5 and β-actin bands for representative samples from this study. **B** Claudin-5/β-actin Peak Area Ratio for each sample in **A**. $p = 0.937$ (Mann–Whitney rank-sum test)

plasma MMP-9 levels at 169.9 ± 39.5 ng/mL ($p = 0.030$; 2.38-fold difference). Plasma MMP-2 levels showed significant associations with CDR scores and Braak staging, whereas plasma MMP-9 levels showed significant associations with MMSE scores in ANOVA analysis (Table 6). Collectively, AD patients had reduced plasma NSE levels, reduced plasma MMP-2, and elevated plasma MMP-9 levels compared to CNI.

Plasma S100β levels for CNI varied from 2.9 pg/mL to 15.2 pg/mL, with average plasma S100β levels at 11.1 ± 2.1 pg/mL (Fig. 9D). In contrast, plasma S100β levels for AD patients were 12.3-fold higher ($p < 0.0001$) with average concentrations at 137.0 ± 8.1 pg/mL in the range of 107.3 pg/mL to 184.4 pg/mL. Generalized linear modeling revealed that plasma S100β levels were higher for patients with severe Braak stages and elevated CDR scores (Table 6; Fig. 9E, F). Plasma S100β levels predict Braak stage II with the highest probability for 0–2 ng/dL, Braak stage III for 2–7 ng/dL, and Braak stage VI for 7–20 ng/dL (Fig. 9E). Plasma S100β levels in the ranges of 0–8 ng/dL, 8–14 ng/dL, and 14–20 ng/dL were more likely to correspond to cases with CDR 0, CDR 0.5, and CDR 3 respectively (Fig. 9F). Increased plasma S100β levels were also associated with increased brain Aβ40 pathology in this cohort (Fig. 9G). These associations were confirmed to be significant by ANOVA analysis (Table 6). However, a visual outlier may be confounding these associations. When modeled excluding this potential outlier (dashed line), the trend was not significant ($p = 0.068$). Bonferroni outlier testing did not exclude this point, and any conclusion should be cautious.

Finally, we assessed the probabilities of each peripheral biomarker to predict different pathological changes in AD (Tables 7, S7-S15). We found that plasma S100β levels provided the highest probability for predicting AD-vs-CNI diagnosis among these biomarkers (Table 7). The remaining pathological and cognitive outcomes did not significantly correlate with circulating biomarker levels (Tables S7-S15). In summary, we found that plasma levels of candidate biomarkers show significant associations with AD pathology and, in the case of S100β, should be tested further as a promising predictor for AD pathology, barrier dysfunction, and cognitive decline in large cohort studies.

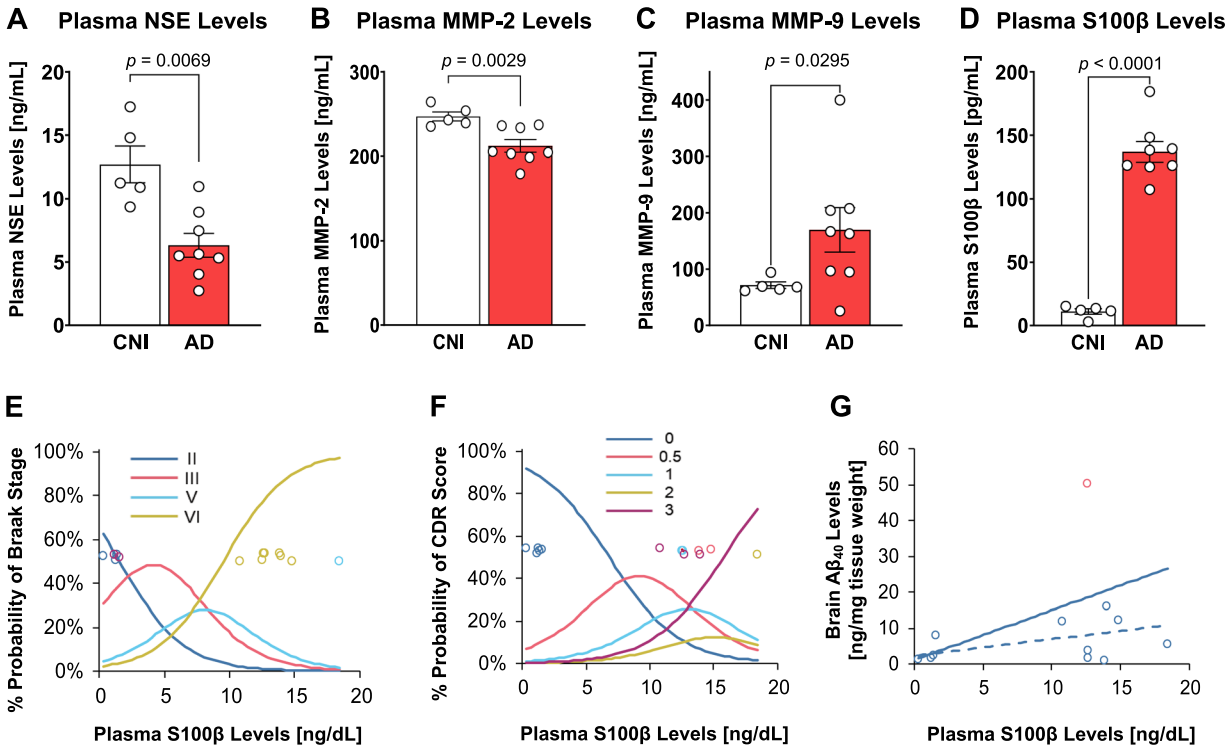

Fig. 9 Peripheral Biomarker Analysis for CNI and AD Patients. **A** Plasma NSE levels (ng/mL) in AD patients and CNI ($p = 0.007$; Welch's *t*-test). **B** Plasma MMP-2 levels (ng/mL) in AD patients and CNI ($p = 0.0029$; Welch's *t*-test). **C** Plasma MMP-9 levels in AD patients and CNI ($p = 0.030$; Mann–Whitney rank-sum test). **D** Plasma S100β levels (pg/mL) in AD patients and CNI ($p < 0.001$; Welch's *t*-test). **E** Plasma S100β levels for different Braak stages (II—blue, III—red, V—light blue, VI—yellow). **F** Plasma S100β levels for different CDR scores (0—blue, 0.5—red, 1—light blue, 2—yellow, 3—magenta). **G** Changes in brain Aβ40 levels in response to changes in plasma S100β levels. A possible visual outlier is indicated in red; the regression line calculated without this point is dashed

Table 6 Variations in peripheral biomarkers with neuropathological, cognitive, and biochemical outcomes for CNI and AD patients

Response	Predictor	Statistic[a]	Raw *p* value	Adjusted *p* value[b]	R^2
Braak stage	Plasma S100β levels (pg/mL)	11.277 (1)	< 0.001	0.008	0.644
Brain $A\beta_{40}$ levels (ng/mg brain tissue)	Plasma S100β levels (pg/mL)	9.899 (1,11)	0.009	0.046	0.406
CDR scores	Plasma MMP-2 levels (ng/mL)	6.609 (1)	0.010	0.046	0.420
Braak stage	Plasma MMP-9 levels (ng/mL)	7.757 (1)	0.005	0.036	0.499

[a] χ^2 or F, as appropriate

[b] Adjusted by Benjamni-Hochberg FDR

Table 7 Model comparisons of peripheral biomarkers vs. consensus diagnosis for CNI and AD patients

Predictor	AICc	Probability[a]	χ2	Raw *p* value	Adjusted *p* value[a]	R^2
Plasma S100β levels (pg/mL)	5.200	0.915	17.323 (1)	< 0.001	0.001	1.000
Plasma NSE levels (ng/mL)	11.918	0.032	10.605 (1)	0.001	0.009	0.637
Plasma MMP-2 levels (ng/mL)	10.994	0.051	11.529 (1)	< 0.001	0.008	0.683
Plasma MMP-9 levels (ng/mL)	16.961	0.003	5.562 (1)	0.018	0.073	0.365

[a] Probability of the model being "correct" vs. other models in set, derived from ΔAICc (Burnham & Anderson, 2002)

[b] Adjusted by Benjamni-Hochberg FDR

Discussion

Blood–brain barrier dysfunction precedes cognitive decline in AD patients, but biomarkers to assess barrier dysfunction and predict AD progression do not exist. We used immunohistochemical, biochemical, and imaging-based methods to examine postmortem tissue samples from 9 CNI and 10 AD patients for Aβ pathology, tau pathology, and blood–brain barrier dysfunction. AD patients in our cohort displayed mild-to-severe cognitive impairment, increased Aβ and tau pathology, and structural changes in the brain. We found minimal changes in microvascular diameters and tight junction protein expression. Analysis of peripheral biomarkers revealed elevated plasma S100β and MMP-9 levels for AD patients compared to CNI. In contrast, plasma levels of NSE and MMP-2 were significantly lower for AD patients when compared with CNI. Evidence from predictive modeling indicated that high plasma S100β levels were predictive for high Braak stage, high CDR score, and elevated Aβ40 brain levels and, thus, could serve as a predictor of AD pathology and cognitive impairment.

AD patients in our cohort had mild-to-severe cognitive impairment, whereas cognition scores for CNI were normal. We found that consensus AD diagnosis and Braak stages were associated with lower MMSE scores ($r = -0.986$) and higher CDR scores ($r = 0.786$). These findings are consistent with previous reports [60, 61]. We found increased Aβ and tau levels in AD brain tissue sections compared to CNI. Immunohistochemical analysis of plaque and tangle pathology markers also showed that AD brain tissue sections had 2- to fourfold higher scores than CNI brain tissue sections. Our data is consistent with previous reports that show twofold higher plaque and tangle pathology in AD patients with severe cognitive impairment when compared to cognitively normal individuals [27, 62]. However, bias in selecting a region of interest is often towards the most severely affected regions [28]. Biochemical analysis of whole brain tissue homogenate provides a non-biased and complementary measurement for immunohistochemical results. Still, biochemical assays may dampen the large inter-cohort differences observed between patient groups [63].

Previous studies indicate that microvascular diameters change with age and disease stage [64, 65]. To determine microvascular diameters in our study, we cleared brain tissue sections and immunostained them for five different markers. However, we found no significant differences in microvascular diameters between capillaries isolated from AD patients versus capillaries from CNI. Multiple research groups have previously used COL-IV as a vascular marker to analyze microvascular diameters in CNI and AD brain tissue sections, but reports are contradictory. For example, Burke et al. [66] found that the microvascular diameters of AD patients ($n = 26$) were 90% of the microvascular diameters of CNI ($n = 14$). In contrast, Hase et al. [67] showed that microvessels in AD patients ($n = 18$) had a 1.8-fold greater diameter compared to microvessels in CNI ($n = 9$). In a third study, Damodarasamy et al. reported that COL-IV diameters in the parietal cortex were similar in AD patients with CAA ($n = 26$) compared to AD patients without CAA ($n = 14$; [68]). Thus, there is a lack of consensus on changes in microvascular diameters in microvessels of AD patients when using COL-IV as a vascular marker. We, therefore, used multiple vascular markers to improve the robustness of our data. We acknowledge, however, that factors such as tissue expansion during tissue clearing, variability in the selected region of interest, quality of immunostaining, and inter-day and inter-person variability can mask subtle differences in microvascular diameters. We also observed that microvascular diameters for fibrinogen-immunostained vessels were smaller than those for COL4-immunostained vessels. We presume the difference is because COL4 stains the outer layer of the vascular basement membrane while vWF and fibrinogen stain blood-borne proteins within the luminal space. We also noted that microvascular diameters for fibrinogen were smallest compared to other vascular markers in this study. Given that fibrinogen is a blood-borne protein expressed outside the central nervous system, it would make sense for fibrinogen diameters to be the smallest and would indicate the luminal space in unperfused brain tissue Sects. [69].

Current literature shows that claudin-5 immunoreactivity is reduced near ruptured vessels or in Aβ-positive capillaries [19, 70]. We did not observe a significant difference in claudin-5 protein expression levels (normalized to β-actin) in isolated capillaries from CNI and AD brain samples. Other factors, such as tissue integrity, post-freeze–thaw cycles, and reduced yield during capillary isolation and lysate extraction, may account for differences in protein levels between groups.

We found lower plasma NSE levels in AD patients compared to CNI. In contrast to our findings, several studies show that plasma levels of NSE do not significantly differ between AD and non-AD samples in large cohort studies [71–73]. Radioimmunoassay analysis of serum NSE levels in a cohort of 24 AD patients and 11 CNI produced similar values (AD 15 ± 7.5 mg/mL; CNI 14 ± 6.5 mg/mL; [72]). Likewise, electrochemiluminescence assay data revealed serum NSE levels to be very close between AD and CNI ($n = 66$; [71]). Data from biochip immunoassays showed that plasma NSE levels were 3.1 ± 7.7 ng/mL for 24 AD patients but 1.9 ± 3.8 for 20 CNI [73]. We conclude that plasma NSE levels can vary depending on detection methods.

MMP-2 (52 kDa) and MMP-9 (92 kDa) are endogenous gelatinases that regulate the remodeling of tight-junction proteins and the extracellular matrix at the blood–brain barrier [74, 75]. Multiple longitudinal studies show that plasma MMP levels increase with disease progression in AD patients [61, 76–79]. We found lower MMP-2 and higher plasma MMP-9 levels for AD patients compared to CNI. Previous reports highlight a lack of consensus on plasma MMP levels analyzed in AD patients and CNI, such as 1.5-fold higher ($p < 0.001$) plasma MMP-9 levels for 24 AD patients (inter-quartile range: 34.4 to 53.7 ng/mL; median: 45.4; $n = 24$) compared to plasma MMP-9 levels for 24 CNI (inter-quartile range: 19.9–39.1 ng/mL; median: 27.0; $n = 24$; [80]). Comparing plasma MMP-9 levels of 95 patients with mild cognitive impairment and 58 CNI indicated no significant differences between the two groups [76]. Plasma MMP-9 levels were even lower in the analysis by Abe and colleagues, i.e., 1.98 ng/mL to 2.28 ng/mL for AD patients and 1.99 ng/mL to 2.28 ng/mL for CNI [76]. Another study reported 1.5-fold lower plasma MMP-9 levels for 25 AD patients (inter-quartile range: 0.93 ng/mL to 8.4 ng/mL; median 5.0 ng/mL) compared to plasma MMP-9 levels for 25 CNI (inter-quartile range: 2.2 ng/mL to 17.5 ng/mL; median: 7.3 ng/mL; [81]). A similar argument can be made for plasma MMP-2 levels. No differences appeared in plasma MMP-2 levels in a cohort of 95 patients with mild cognitive impairment and 95 CNI and ranged from 3.5 ng/mL to 3.7 ng/mL (inter-quartile range; [76]). However, these data are opposite to data presented by Tuna et al. [82] showing 2.8-fold lower ($p = 0.002$) plasma MMP-2 levels for 30 AD patients (inter-quartile range: 1.6–19.0 ng/mL; median: 13.8 ng/mL) when compared to plasma MMP-2 levels for 30 CNI (inter-quartile range: 12.1–83.3 ng/mL; median: 38.6 ng/mL). Plasma MMP levels can vary dramatically based on the analytical method and chosen cohorts. Overall, it appears that MMP levels have high variability among AD cases [83]. A systematic analysis of these analytes across all studies that accounts for the severity of AD pathology and demographic differences, such as sex or age, is lacking and may provide more insights into the utility of MMPs as peripheral biomarkers.

Our data show a significant increase in plasma S100β levels in AD patients and suggest that plasma S100β could be a promising predictor for cognitive impairment, Braak staging, and brain Aβ40 pathology. Our findings align with previous reports highlighting that increased S100β levels correlate with cognitive impairment. Serum S100β levels determined by ELISA in a cohort of 100 AD patients and 100 age- and sex-matched healthy controls were elevated in AD patients with CDR scores of 2 and 3 [84]. Serum S100β levels likewise increased with CDR scores in a cohort of 54 AD patients and 66 CNI [71]. The plasma S100β levels in our study are lower than those observed in stroke and patients with epilepsy, both disorders that go along with severe blood–brain barrier dysfunction [85–87]. Our data and data from previous reports indicate that the association between peripheral S100β levels and cognition is consistently observed across studies. In addition, S100β is well-established as a biomarker for acute neuronal and glial injury in disorders that include stroke, epilepsy, traumatic brain injury (TBI), and concussion [88–90]. In neurodegenerative conditions, serum S100β levels correlate with disease severity in Parkinson's disease [91] but not in amyotrophic lateral sclerosis [92]. However, a systematic review is still needed to accurately contrast S100β levels with disease severity across various proteinopathies.

Conclusions

Our data suggest plasma S100β levels could be a promising predictor for cognitive impairment, Braak staging, and brain Aβ40 pathology. Although promising, we suggest that no single biomarker would likely be reliable enough to predict the progression of AD pathology and cognitive decline. We presume a panel of multiple biomarkers would be more sensitive and robust. Further investigation is necessary to validate plasma S100β levels as a predictor for barrier dysfunction, dementia severity, and AD pathology in large patient cohorts.

Abbreviations

AD	Alzheimer's disease
AICc	Akaike information criterion (AIC) with a correction for small sample sizes
ANOVA	Analysis of variance
APOE	Apolipoprotein E
Aβ	Amyloid-β
BSA	Bovine serum albumin
CA	Cortical atrophy
CAA	Cerebral amyloid angiopathy
CDR	Clinical dementia rating
CNI	Cognitively normal individuals
COL-IV	Collagen-IV
DP	Diffused plaques
GFAP	Glial fibrillary acidic protein
GLUT-1	Glucose transporter 1
IRB	Institutional review board
MIP	Maximum intensity projection
MMP	Matrix metalloproteinase
MMSE	Mini-mental state examination
MRI	Magnetic resonance imaging
NFT	Neurofibrillary tangles
NP	Neuritic plaques
NSE	Neuron-specific enolase
PBS	Phosphate buffered saline
PDGFRβ	Platelet-derived growth factor receptor beta
S100β	S100 beta
UK-ADC	University of Kentucky Alzheimer's Disease Center
VCAM-1	Vascular cell adhesion molecule-1
vWF	Von Willebrand factor
ZO-1	Zonula occludens-1

Supplementary Information

The online version contains supplementary material available at https://doi.org/10.1186/s12987-024-00615-8.

Supplementary Material 1. Fig. S1 Associations between GFAP Intensity and Pathological Outcomes in this Study. Fig. S2 Associations between Microvascular PDGFRβ Diameter and Pathological Outcomes. Fig. S3 Associations between Microvascular COL-IV Diameter and Pathological Outcomes. Fig. S4 Associations between Microvascular vWF Diameter and Pathological Outcomes. Fig. S5 Associations between Microvascular GLUT-1 Diameter and Pathological Outcomes. Fig. S6 Associations between Microvascular Fibrinogen Diameter and Pathological Outcomes.

Acknowledgements
The authors acknowledge current and former members of the Bauer and Hartz laboratories for proofreading the manuscript. We also acknowledge Ms. Sonya Anderson for providing human brain tissue and plasma samples from the UK-ADC core and Ms. Amy Joubert for assistance with ELISA assays.

Author contributions
GN generated and analyzed the data, drafted the outline, wrote the first draft, and revised the manuscript. AH, EA, RS, PN, BM, and BB contributed to the experimental design, sample preparation, data analysis and interpretation, and revised the manuscript. WC analyzed confocal imaging data. EA and PN provided the UK-ADC core patient datasets and plasma and brain tissue samples. BM performed statistical, modeling, and correlation analyses for the entire dataset and revised the manuscript. All authors were involved in drafting and revising the manuscript. All authors approved the final version and agreed to be accountable for all aspects of the work, ensuring that questions related to the accuracy or integrity of any part of the work are appropriately investigated and resolved.

Funding
The funding for this study was provided by the National Institute of Health (Grant 2R01AG039621, PI: Hartz; R01AG075583, MPI: Hartz, Bauer; R01NS133250, PI: Hartz). Digital slide scanning efforts were supported by UK-ADC P30 grant (AG072946).

Availability of data and materials
The datasets used and/or analyzed in the current study are available from the corresponding author upon reasonable request.

Declarations

Ethics approval and consent to participate
The Human Research/Institutional Review Board (IRB) at the University of Kentucky (#B18-3115-M4) approved all experiments involving human tissue samples.

Consent for publication
Not applicable.

Competing interests
The authors declare that the research was conducted without any commercial or financial relationships that could be construed as a potential conflict of interest.

Author details
[1]Sanders-Brown Center on Aging, College of Medicine, University of Kentucky, 760 Press Ave, 124 HKRB, Lexington, KY 40536-0679, USA. [2]Department of Biostatistics, College of Public Health, University of Kentucky, Lexington, USA. [3]Department of Epidemiology and Environmental Health, College of Public Health, University of Kentucky, Lexington, USA. [4]Department of Pathology, College of Medicine, University of Kentucky, Lexington, USA. [5]Department of Pharmaceutical Sciences, College of Pharmacy, University of Kentucky, Lexington, USA. [6]Department of Pharmacology and Nutritional Sciences, College of Medicine, University of Kentucky, Lexington, USA.

Received: 14 August 2024 Accepted: 20 December 2024
Published online: 09 January 2025

References

1. Cummings JL, Osse AML, Kinney JW. Alzheimer's disease: novel targets and investigational drugs for disease modification. Drugs. 2023;83(15):1387–408.
2. Hampel H, Cummings J, Blennow K, Gao P, Jack CR Jr, Vergallo A. Developing the ATX(N) classification for use across the Alzheimer disease continuum. Nat Rev Neurol. 2021;17(9):580–9.
3. Nehra G, Bauer B, Hartz AMS. Blood-brain barrier leakage in Alzheimer's disease: from discovery to clinical relevance. Pharmacol Ther. 2022;234:108119.
4. Di Santo SG, Prinelli F, Adorni F, Caltagirone C, Musicco M. A meta-analysis of the efficacy of donepezil, rivastigmine, galantamine, and memantine in relation to severity of Alzheimer's disease. J Alzheimers Dis. 2013;35(2):349–61.
5. Sevigny J, Chiao P, Bussiere T, Weinreb PH, Williams L, Maier M, et al. The antibody aducanumab reduces Abeta plaques in Alzheimer's disease. Nature. 2016;537(7618):50–6.
6. van Dyck CH, Swanson CJ, Aisen P, Bateman RJ, Chen C, Gee M, et al. Lecanemab in early Alzheimer's disease. N Engl J Med. 2023;388(1):9–21.
7. Budd Haeberlein S, Aisen PS, Barkhof F, Chalkias S, Chen T, Cohen S, et al. Two randomized phase 3 studies of aducanumab in early Alzheimer's disease. J Prev Alzheimer Dis. 2022;9(2):197–210.
8. Swanson CJ, Zhang Y, Dhadda S, Wang J, Kaplow J, Lai RYK, et al. A randomized, double-blind, phase 2b proof-of-concept clinical trial in early Alzheimer's disease with lecanemab, an anti-Abeta protofibril antibody. Alzheimers Res Ther. 2021;13(1):80.
9. Jack CR, Wiste HJ, Algeciras-Schimnich A, Figdore DJ, Schwarz CG, Lowe VJ, et al. Predicting amyloid PET and tau PET stages with plasma biomarkers. Brain. 2023;146(5):2029–44.
10. Moon WJ, Lim C, Ha IH, Kim Y, Moon Y, Kim HJ, et al. Hippocampal blood-brain barrier permeability is related to the APOE4 mutation status of elderly individuals without dementia. J Cereb Blood Flow Metab. 2021;41(6):1351–61.
11. Uchida Y, Kan H, Sakurai K, Oishi K, Matsukawa N. Contributions of blood-brain barrier imaging to neurovascular unit pathophysiology of Alzheimer's disease and related dementias. Front Aging Neurosci. 2023;15:1111448.
12. Akkaya BG, Zolnerciks JK, Ritchie TK, Bauer B, Hartz AM, Sullivan JA, et al. The multidrug resistance pump ABCB1 is a substrate for the ubiquitin ligase NEDD4-1. Mol Membr Biol. 2015;32(2):39–45.
13. Andjelkovic AV, Situ M, Citalan-Madrid AF, Stamatovic SM, Xiang J, Keep RF. Blood-brain barrier dysfunction in normal aging and neurodegeneration: mechanisms, impact, and treatments. Stroke. 2023;54(3):661–72.
14. Carrano A, Hoozemans JJ, van der Vies SM, van Horssen J, de Vries HE, Rozemuller AJ. Neuroinflammation and blood-brain barrier changes in capillary amyloid angiopathy. Neurodegener Dis. 2012;10(1–4):329–31.
15. Chai AB, Hartz AMS, Gao X, Yang A, Callaghan R, Gelissen IC. New evidence for P-gp-mediated export of amyloid-β PEPTIDES in molecular, blood-brain barrier and neuronal models. Int J Mol Sci. 2020. https://doi.org/10.3390/ijms22010246.
16. Lee J, Yanckello LM, Ma D, Hoffman JD, Parikh I, Thalman S, et al. Neuroimaging biomarkers of mTOR inhibition on vascular and metabolic functions in aging brain and Alzheimer's disease. Front Aging Neurosci. 2018;10:225.
17. Lin AL, Parikh I, Yanckello LM, White RS, Hartz AMS, Taylor CE, et al. APOE genotype-dependent pharmacogenetic responses to rapamycin for preventing Alzheimer's disease. Neurobiol Dis. 2020;139: 104834.
18. Nation DA, Sweeney MD, Montagne A, Sagare AP, D'Orazio LM, Pachicano M, et al. Blood-brain barrier breakdown is an early biomarker of human cognitive dysfunction. Nat Med. 2019;25(2):270–6.
19. Viggars AP, Wharton SB, Simpson JE, Matthews FE, Brayne C, Savva GM, et al. Alterations in the blood brain barrier in ageing cerebral cortex in relationship to Alzheimer-type pathology: a study in the MRC-CFAS population neuropathology cohort. Neurosci Lett. 2011;505(1):25–30.
20. Hartz AM, Bauer B, Soldner EL, Wolf A, Boy S, Backhaus R, et al. Amyloid-β contributes to blood-brain barrier leakage in transgenic

human amyloid precursor protein mice and in humans with cerebral amyloid angiopathy. Stroke. 2012;43(2):514–23.
21. Scheibel AB. Alterations of the cerebral capillary bed in the senile dementia of Alzheimer. Ital J Neurol Sci. 1987;8(5):457–63.
22. Kurz C, Walker L, Rauchmann BS, Perneczky R. Dysfunction of the blood-brain barrier in Alzheimer's disease: evidence from human studies. Neuropathol Appl Neurobiol. 2022;48(3): e12782.
23. Schmitt FA, Nelson PT, Abner E, Scheff S, Jicha GA, Smith C, et al. University of Kentucky Sanders-brown healthy brain aging volunteers: donor characteristics, procedures and neuropathology. Curr Alzheimer Res. 2012;9(6):724–33.
24. Abner EL, Kryscio RJ, Schmitt FA, Santacruz KS, Jicha GA, Lin Y, et al. "End-stage" neurofibrillary tangle pathology in preclinical Alzheimer's disease: fact or fiction? J Alzheimers Dis. 2011;25(3):445–53.
25. Byrne UT, Ross JM, Faull RL, Dragunow M. High-throughput quantification of Alzheimer's disease pathological markers in the post-mortem human brain. J Neurosci Methods. 2009;176(2):298–309.
26. Lamy C, Duyckaerts C, Delaere P, Payan C, Fermanian J, Poulain V, et al. Comparison of seven staining methods for senile plaques and neurofibrillary tangles in a prospective series of 15 elderly patients. Neuropathol Appl Neurobiol. 1989;15(6):563–78.
27. Nelson PT, Braak H, Markesbery WR. Neuropathology and cognitive impairment in Alzheimer disease: a complex but coherent relationship. J Neuropathol Exp Neurol. 2009;68(1):1–14.
28. Nelson PT, Jicha GA, Schmitt FA, Liu H, Davis DG, Mendiondo MS, et al. Clinicopathologic correlations in a large Alzheimer disease center autopsy cohort: neuritic plaques and neurofibrillary tangles "do count" when staging disease severity. J Neuropathol Exp Neurol. 2007;66(12):1136–46.
29. D'Andrea MR, Nagele RG. Morphologically distinct types of amyloid plaques point the way to a better understanding of Alzheimer's disease pathogenesis. Biotech Histochem. 2010;85(2):133–47.
30. Liu F, Sun J, Wang X, Jin S, Sun F, Wang T, et al. Focal-type, but not diffuse-type, amyloid beta plaques are correlated with Alzheimer's neuropathology, cognitive dysfunction, and neuroinflammation in the human hippocampus. Neurosci Bull. 2022;38(10):1125–38.
31. Helman AM, Siever M, McCarty KL, Lott IT, Doran E, Abner EL, et al. Microbleeds and cerebral amyloid angiopathy in the brains of people with down syndrome with Alzheimer's disease. J Alzheimers Dis. 2019;67(1):103–12.
32. Olichney JM, Hansen LA, Hofstetter CR, Lee JH, Katzman R, Thal LJ. Association between severe cerebral amyloid angiopathy and cerebrovascular lesions in Alzheimer disease is not a spurious one attributable to apolipoprotein E4. Arch Neurol. 2000;57(6):869–74.
33. Vonsattel JP, Myers RH, Hedley-Whyte ET, Ropper AH, Bird ED, Richardson EP Jr. Cerebral amyloid angiopathy without and with cerebral hemorrhages: a comparative histological study. Ann Neurol. 1991;30(5):637–49.
34. Besser L, Kukull W, Knopman DS, Chui H, Galasko D, Weintraub S, et al. Version 3 of the national Alzheimer's coordinating center's uniform data set. Alzheimer Dis Assoc Disord. 2018;32(4):351–8.
35. Bellaver B, Ferrari-Souza JP, Uglione da Ros L, Carter SF, Rodriguez-Vieitez E, Nordberg A, et al. Astrocyte biomarkers in Alzheimer disease: a systematic review and meta-analysis. Neurology. 2021;96(24):e2944–55.
36. Kim KY, Shin KY, Chang KA. GFAP as a potential biomarker for Alzheimer's disease: a systematic review and meta-analysis. Cells. 2023. https://doi.org/10.3390/cells12091309.
37. Steiner J, Bogerts B, Schroeter ML, Bernstein HG. S100B protein in neurodegenerative disorders. Clin Chem Lab Med. 2011;49(3):409–24.
38. Verkerke M, Hol EM, Middeldorp J. Physiological and pathological ageing of astrocytes in the human brain. Neurochem Res. 2021;46(10):2662–75.
39. Viejo L, Noori A, Merrill E, Das S, Hyman BT, Serrano-Pozo A. Systematic review of human post-mortem immunohistochemical studies and bioinformatics analyses unveil the complexity of astrocyte reaction in Alzheimer's disease. Neuropathol Appl Neurobiol. 2022;48(1): e12753.
40. Hartz AMS, Rempe RG, Soldner ELB, Pekcec A, Schlichtiger J, Kryscio R, et al. Cytosolic phospholipase A2 is a key regulator of blood-brain barrier function in epilepsy. Faseb J. 2019;33(12):14281–95.
41. Hartz AMS, Zhong Y, Shen AN, Abner EL, Bauer B. Preventing P-gp ubiquitination lowers Aβ brain levels in an Alzheimer's disease mouse model. Front Aging Neurosci. 2018;10:186.
42. Soldner ELB, Hartz AMS, Akanuma SI, Pekcec A, Doods H, Kryscio RJ, et al. Inhibition of human microsomal PGE2 synthase-1 reduces seizure-induced increases of P-glycoprotein expression and activity at the blood-brain barrier. Faseb J. 2019;33(12):13966–81.
43. Sziraki A, Zhong Y, Neltner AM, Niedowicz DM, Rogers CB, Wilcock DM, et al. A high-throughput single-cell RNA expression profiling method identifies human pericyte markers. Neuropathol Appl Neurobiol. 2023;49(6): e12942.
44. Ding Y, Zhong Y, Baldeshwiler A, Abner EL, Bauer B, Hartz AMS. Protecting P-glycoprotein at the blood-brain barrier from degradation in an Alzheimer's disease mouse model. Fluids Barriers CNS. 2021;18(1):10.
45. Nehra G, Promsan S, Yubolphan R, Chumboatong W, Vivithanaporn P, Maloney BJ, et al. Cognitive decline, Abeta pathology, and blood-brain barrier function in aged 5xFAD mice. Fluids Barriers CNS. 2024;21(1):29.
46. Vulin M, Zhong Y, Maloney BJ, Bauer B, Hartz AMS. Proteasome inhibition protects blood-brain barrier P-glycoprotein and lowers Aβ brain levels in an Alzheimer's disease model. Fluids Barriers CNS. 2023;20(1):70.
47. Bradford MM. A rapid and sensitive method for the quantitation of microgram quantities of protein utilizing the principle of protein-dye binding. Anal Biochem. 1976;72:248–54.
48. Hartz AM, Pekcec A, Soldner EL, Zhong Y, Schlichtiger J, Bauer B. P-gp protein expression and transport activity in rodent seizure models and human epilepsy. Mol Pharm. 2017;14(4):999–1011.
49. Hartz AM, Zhong Y, Wolf A, LeVine H 3rd, Miller DS, Bauer B. Aβ40 reduces P-glycoprotein at the blood-brain barrier through the ubiquitin-proteasome pathway. J Neurosci. 2016;36(6):1930–41.
50. Team RC. R: a language and environment for statistical computing, R foundation for statistical computing. https://www.r-projectorg/.
51. Fox J. Polycor: polychoric and polyserial correlations. 2022. https://www.cranr-projectorg/web/packages/polycor/indexhtml.
52. Benjamini Y, Drai D, Elmer G, Kafkafi N, Golani I. Controlling the false discovery rate in behavior genetics research. Behav Brain Res. 2001;125(1–2):279–84.
53. Bates D, Mächler M, Bolker B, Walker S. Fitting linear mixed-effects models using lme4. J Stat Softw. 2015;67(1):1–48.
54. Nakagawa S, Johnson PCD, Schielzeth H. The coefficient of determination R2 and intra-class correlation coefficient from generalized linear mixed-effects models revisited and expanded. J R Soc Interfac. 2017. https://doi.org/10.1098/rsif.2017.0213.
55. Christensen RHB. Regression models for ordinal data: introducing R-package ordinal. 2022. https://www.CRAN.R-project.org/package=ordinal.
56. Burnham KP, Anderson DR. Model selection and multimodel inference: a practical information-theoretic approach. 2nd ed. New York: Springer; 2002. p. 488.
57. Nagelkerke NJD. A note on a general definition of the coefficient of determination. Biometrika. 1991;78(3):691–2.
58. Tjur T. Coefficients of determination in logistic regression models—a new proposal: the coefficient of discrimination. Am Stat. 2009;63(4):366–72.
59. Olejnik S, Algina J. Generalized eta and omega squared statistics: measures of effect size for some common research designs. Psychol Method. 2003;8(4):434–47.
60. Perneczky R, Wagenpfeil S, Komossa K, Grimmer T, Diehl J, Kurz A. Mapping scores onto stages: mini-mental state examination and clinical dementia rating. Am J Geriatr Psychiatry. 2006;14(2):139–44.
61. Tsiknia AA, Edland SD, Sundermann EE, Reas ET, Brewer JB, Galasko D, et al. Sex differences in plasma p-tau181 associations with Alzheimer's disease biomarkers, cognitive decline, and clinical progression. Mol Psychiatry. 2022;27(10):4314–22.
62. Loeffler DA, Camp DM, Bennett DA. Plaque complement activation and cognitive loss in Alzheimer's disease. J Neuroinflammation. 2008;5:9.
63. Ferrier CM, de Witte HH, Straatman H, van Tienoven DH, van Geloof WL, Rietveld FJ, et al. Comparison of immunohistochemistry with immunoassay (ELISA) for the detection of components of the plasminogen activation system in human tumour tissue. Br J Cancer. 1999;79(9–10):1534–41.
64. Merlini M, Wanner D, Nitsch RM. Tau pathology-dependent remodelling of cerebral arteries precedes Alzheimer's disease-related microvascular cerebral amyloid angiopathy. Acta Neuropathol. 2016;131(5):737–52.

65. Stopa EG, Butala P, Salloway S, Johanson CE, Gonzalez L, Tavares R, et al. Cerebral cortical arteriolar angiopathy, vascular beta-amyloid, smooth muscle actin, Braak stage, and APOE genotype. Stroke. 2008;39(3):814–21.
66. Burke MJ, Nelson L, Slade JY, Oakley AE, Khundakar AA, Kalaria RN. Morphometry of the hippocampal microvasculature in post-stroke and age-related dementias. Neuropathol Appl Neurobiol. 2014;40(3):284–95.
67. Hase Y, Ding R, Harrison G, Hawthorne E, King A, Gettings S, et al. White matter capillaries in vascular and neurodegenerative dementias. Acta Neuropathol Commun. 2019;7(1):16.
68. Damodarasamy M, Vernon RB, Pathan JL, Keene CD, Day AJ, Banks WA, et al. The microvascular extracellular matrix in brains with Alzheimer's disease neuropathologic change (ADNC) and cerebral amyloid angiopathy (CAA). Fluid Barriers CNS. 2020;17(1):60.
69. Petersen MA, Ryu JK, Akassoglou K. Fibrinogen in neurological diseases: mechanisms, imaging and therapeutics. Nat Rev Neurosci. 2018;19(5):283–301.
70. Simpson JE, Ince PG, Lace G, Forster G, Shaw PJ, Matthews F, et al. Astrocyte phenotype in relation to Alzheimer-type pathology in the ageing brain. Neurobiol Aging. 2010;31(4):578–90.
71. Chaves ML, Camozzato AL, Ferreira ED, Piazenski I, Kochhann R, Dall'Igna O, et al. Serum levels of S100B and NSE proteins in Alzheimer's disease patients. J Neuroinflammation. 2010;7:6.
72. Parnetti L, Palumbo B, Cardinali L, Loreti F, Chionne F, Cecchetti R, et al. Cerebrospinal fluid neuron-specific enolase in Alzheimer's disease and vascular dementia. Neurosci Lett. 1995;183(1–2):43–5.
73. Rosen C, Mattsson N, Johansson PM, Andreasson U, Wallin A, Hansson O, et al. Discriminatory analysis of biochip-derived protein patterns in CSF and plasma in neurodegenerative diseases. Front Aging Neurosci. 2011;3:1.
74. Rempe RG, Hartz AMS, Bauer B. Matrix metalloproteinases in the brain and blood-brain barrier: versatile breakers and makers. J Cereb Blood Flow Metab. 2016;36(9):1481–507.
75. Rempe RG, Hartz AMS, Soldner ELB, Sokola BS, Alluri SR, Abner EL, et al. Matrix metalloproteinase-mediated blood-brain barrier dysfunction in epilepsy. J Neurosci. 2018;38(18):4301–15.
76. Abe K, Chiba Y, Hattori S, Yoshimi A, Asami T, Katsuse O, et al. Influence of plasma matrix metalloproteinase levels on longitudinal changes in Alzheimer's disease (AD) biomarkers and cognitive function in patients with mild cognitive impairment due to AD registered in the Alzheimer's disease neuroimaging initiative database. J Neurol Sci. 2020;416: 116989.
77. Benoit JS, Chan W, Piller L, Doody R. Longitudinal sensitivity of Alzheimer's disease severity staging. Am J Alzheimers Dis Other Demen. 2020;35:1533317520918719.
78. Iulita MF, Ganesh A, Pentz R, Flores Aguilar L, Gubert P, Ducatenzeiler A, et al. Identification and preliminary validation of a plasma profile associated with cognitive decline in dementia and at-risk individuals: a retrospective cohort analysis. J Alzheimers Dis. 2019;67(1):327–41.
79. Whelan CD, Mattsson N, Nagle MW, Vijayaraghavan S, Hyde C, Janelidze S, et al. Multiplex proteomics identifies novel CSF and plasma biomarkers of early Alzheimer's disease. Acta Neuropathol Commun. 2019;7(1):169.
80. Liu J, Li X, Qu J. Plasma MMP-9/TIMP-1 ratio serves as a novel potential biomarker in Alzheimer's disease. NeuroReport. 2023;34(15):767–72.
81. Koca S, Kiris I, Sahin S, Cinar N, Karsidag S, Hanagasi HA, et al. Decreased levels of cytokines implicate altered immune response in plasma of moderate-stage Alzheimer's disease patients. Neurosci Lett. 2022;786: 136799.
82. Tuna G, Yener GG, Oktay G, İşlekel GH, Kİrkalİ FG. Evaluation of matrix metalloproteinase-2 (MMP-2) and -9 (MMP-9) and their tissue inhibitors (TIMP-1 and TIMP-2) in plasma from patients with neurodegenerative dementia. J Alzheimers Dis. 2018;66(3):1265–73.
83. Radosinska D, Radosinska J. The link between matrix metalloproteinases and Alzheimer's disease pathophysiology. Mol Neurobiol. 2024. https://doi.org/10.1007/s12035-024-04315-0.
84. Chaudhuri JR, Mridula KR, Rathnakishore C, Anamika A, Samala NR, Balaraju B, et al. Association serum S100B protein in Alzheimer's disease: a case control study from South India. Curr Alzheimer Res. 2020;17(12):1095–101.
85. Kaciński M, Budziszewska B, Lasoń W, Zając A, Skowronek-Bała B, Leśkiewicz M, et al. Level of S100B protein, neuron specific enolase, orexin A, adiponectin and insulin-like growth factor in serum of pediatric patients suffering from sleep disorders with or without epilepsy. Pharmacol Rep. 2012;64(6):1427–33.
86. Lasek-Bal A, Jedrzejowska-Szypulka H, Student S, Warsz-Wianecka A, Zareba K, Puz P, et al. The importance of selected markers of inflammation and blood-brain barrier damage for short-term ischemic stroke prognosis. J Physiol Pharmacol. 2019. https://doi.org/10.6402/jpp.2019.2.04.
87. Montaner J, Mendioroz M, Delgado P, García-Berrocoso T, Giralt D, Merino C, et al. Differentiating ischemic from hemorrhagic stroke using plasma biomarkers: the S100B/RAGE pathway. J Proteomics. 2012;75(15):4758–65.
88. Onatsu J, Vanninen R, Jäkälä P, Mustonen P, Pulkki K, Korhonen M, et al. Tau, S100B and NSE as blood biomarkers in acute cerebrovascular events. In Vivo. 2020;34(5):2577–86.
89. Abboud T, Rohde V, Mielke D. Mini review: current status and perspective of S100B protein as a biomarker in daily clinical practice for diagnosis and prognosticating of clinical outcome in patients with neurological diseases with focus on acute brain injury. BMC Neurosci. 2023;24(1):38.
90. Kozlowski T, Bargiel W, Grabarczyk M, Skibinska M. Peripheral S100B protein levels in five major psychiatric disorders: a systematic review. Brain Sci. 2023. https://doi.org/10.3390/brainsci13091334.
91. Angelopoulou E, Paudel YN, Piperi C. Emerging role of S100B protein implication in Parkinson's disease pathogenesis. Cell Mol Life Sci. 2021;78(4):1445–53.
92. Cao MC, Cawston EE, Chen G, Brooks C, Douwes J, McLean D, et al. Serum biomarkers of neuroinflammation and blood-brain barrier leakage in amyotrophic lateral sclerosis. BMC Neurol. 2022;22(1):216.

Publisher's Note